New Journal of Physics
The open-access journal for physics

Atmospheric neutrinos

Takaaki Kajita
Research Center for Cosmic Neutrinos, Institute for Cosmic Ray Research, University of Tokyo, Kashiwa-no-ha 5-1-5, Kashiwa, Chiba 277-8582, Japan
E-mail: kajita@icrr.u-tokyo.ac.jp

New Journal of Physics **6** (2004) 194
Received 23 August 2004
Published 10 December 2004
Online at http://www.njp.org/
doi:10.1088/1367-2630/6/1/194

Abstract. Neutrino oscillation was discovered through the study of atmospheric neutrinos. Atmospheric neutrinos are produced as decay products in hadronic showers resulting from collisions of cosmic rays with nuclei in the atmosphere. Electron neutrinos and muon neutrinos are produced mainly by the decay chain of charged pions to muons and electrons. Depending on the energy of the neutrinos, atmospheric neutrinos are observed as fully contained events, partially contained events and upward-going muon events. The energy range covered by these events is from a few hundred MeV to >1 TeV. Data from various experiments showed zenith angle- and energy-dependent deficit of ν_μ events, while ν_e events did not show any such effect. It was also shown that the ν_μ survival probability obeys the sinusoidal function as predicted by neutrino oscillations. Two-flavour $\nu_\mu \leftrightarrow \nu_\tau$ oscillations, with $\sin^2 2\theta > 0.90$ and Δm^2 in the region of 1.9×10^{-3} to 3.0×10^{-3} eV^2, explain all these data. Various detailed studies using high statistics atmospheric neutrino data excluded the alternative hypotheses that were proposed to explain the ν_μ deficit.

PII: S1367-2630(04)85325-4

Contents

1. Introduction

Studies of the neutrino have played essential roles in the understanding of elementary particle physics. In the standard model of elementary particle physics, neutrinos have been assumed to have zero mass. It has been recognized that the small but finite neutrino masses can be understood naturally by the see-saw mechanism [1, 2] by introducing super-heavy neutral particles. The neutrino mass inferred from atmospheric and other experiments suggests that the mass of the super-heavy neutral particle could be close to the energy scale of the Grand Unification [3, 4]. Therefore, it is widely understood that an experimental study of neutrino masses and mixing angles is one of the few ways to explore physics beyond the standard model, especially physics at the Grand Unification scale.

One of the most sensitive methods to observe small neutrino masses is to study neutrino flavour oscillations [5, 6]. If neutrinos have a finite mass, each flavour eigenstate (for example, ν_μ) can be expressed by a combination of mass eigenstates (ν_1, ν_2 and ν_3). The relation between the

mass eigenstates (ν_1, ν_2, ν_3) and the flavour eigenstates (ν_e, ν_μ, ν_τ) can be expressed by

$$\begin{pmatrix} \nu_e \\ \nu_\mu \\ \nu_\tau \end{pmatrix} = U \begin{pmatrix} \nu_1 \\ \nu_2 \\ \nu_3 \end{pmatrix}, \tag{1}$$

where U is the mixing matrix. This matrix is often called the MNSP (or MNS, or PMNS) matrix taking the initials of the authors who discussed neutrino oscillations for the first time [5, 6]. For simplicity, let us discuss two-flavour neutrino oscillations. The probability for a neutrino produced in a flavour state ν_α to be observed in a flavour state ν_β after travelling a distance L through the vacuum is:

$$P(\nu_\alpha \to \nu_\beta) = \sin^2 2\theta \sin^2 \left(\frac{1.27 \Delta m^2(\mathrm{eV}^2) L(\mathrm{km})}{E_\nu(\mathrm{GeV})} \right), \tag{2}$$

where E_ν is the neutrino energy, θ is the mixing angle between the flavour eigenstates and mass eigenstates and Δm^2 is the mass-squared difference of the neutrino mass eigenstates.

The above description has to be generalized to three-flavour oscillations. In the three-flavour oscillation framework, neutrino oscillations are parametrized by three mixing angles (θ_{12}, θ_{23} and θ_{13}), three mass-squared differences (Δm^2_{12}, Δm^2_{23} and Δm^2_{13}; of the three Δm^2's, only two are independent) and one CP phase (δ). In this case, the mixing matrix U is expressed by

$$U = \begin{pmatrix} c_{12}c_{13} & s_{12}c_{13} & s_{13}e^{-i\delta} \\ -s_{12}c_{23} - c_{12}s_{23}s_{13}e^{i\delta} & c_{12}c_{23} - s_{12}s_{23}s_{13}e^{i\delta} & s_{23}c_{13} \\ s_{12}s_{23} - c_{12}c_{23}s_{13}e^{i\delta} & -c_{12}s_{23} - s_{12}c_{23}s_{13}e^{i\delta} & c_{23}c_{13} \end{pmatrix}, \tag{3}$$

where c_{ij} and s_{ij} represent $\cos\theta_{ij}$ and $\sin\theta_{ij}$, respectively. See, e.g., [7] for more detailed discussions on the neutrino mixing.

If a neutrino mass hierarchy is assumed, the three Δm^2's are approximated by two Δm^2's, and neutrino oscillation lengths are significantly different for the two Δm^2's. One $\Delta m^2 (\Delta m^2_{12})$ is related to solar neutrino experiments and the KamLAND reactor experiment. The other Δm^2 (Δm^2_{23} or Δm^2_{13}) is related to atmospheric, reactor and long-baseline neutrino oscillation experiments. It is known that it is approximately correct to assume two-flavour oscillations for analyses of the present neutrino oscillation data. Therefore, in this paper, we mostly discuss two-flavour neutrino oscillations assuming two significantly different Δm^2's.

Atmospheric neutrinos arise from the decay of secondaries (π, K and μ) produced by primary cosmic ray interactions in the atmosphere. These neutrinos can be detected by underground neutrino detectors. Interactions of low-energy neutrinos, around 1 GeV, have all of the final state particles 'fully contained (FC)' in the detector. Higher energy charged current ν_μ interactions may result in the muon exiting the detector; these are referred to as 'partially contained (PC)'. In order to reject the background from cosmic ray particles, as well as to cleanly reconstruct the details of the event, the vertex position of the interaction is typically defined to be within some fiducial volume. In addition, some of the detectors are equipped with outer detectors (also referred to as veto- or anti-detectors) to easily identify penetrating particles.

There is a third category of charged current ν_μ events, where the interaction occurs outside the detector, and the muon enters and either passes through the detector or stops in the detector.

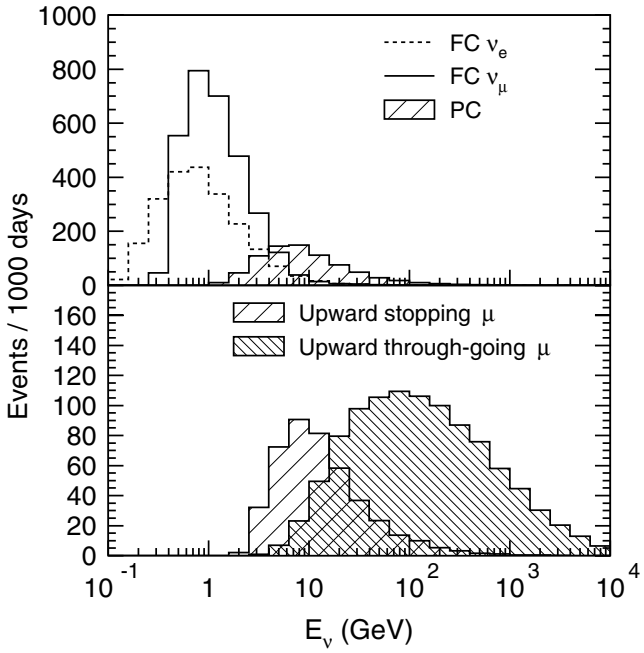

Figure 1. The parent neutrino energy distributions for several different classifications of atmospheric neutrino events. These distributions are for the Super-Kamiokande analysis; for other detectors they will be similar but different depending on detector size, which controls the maximum energy of a fully contained event and the minimum energy of a through-going muon.

These are referred to as 'upward-going muons' because one generally requires that they originate from below the horizon to ensure that a sufficient amount of rock absorbs ordinary cosmic ray muons. Each of the fully contained partially contained and upward-going muon event samples has a certain range of parent neutrino energies. As an example, figure 1 shows the distribution of parent neutrino energies for each category of event samples for the Super-Kamiokande analysis. The energies of atmospheric neutrinos observed in underground detectors range from about 100 MeV to >1 TeV.

Atmospheric neutrino experiments started in the 1960s. One experiment was carried out in the Kolar Gold Field in India [8]. Other experiments were carried out at the East Rand Proprietary Mine in South Africa [9, 10]. In all these experiments, neutrino events occurring in the rock surrounding a neutrino detector were measured. Since the experiments were carried out in extremely deep underground (about 8000 metres water equivalent (m.w.e.)), the charged particles traversing the detectors almost horizontally were essentially of atmospheric neutrino origin. Also, since it was required that the particle should penetrate through the rock and the detector, most of these neutrinos were expected to be charged current (CC) ν_μ events.

In the early 1980s, the first massive underground detectors (of the order of 1 kt) were constructed, primarily to search for proton decay with a lifetime of less than 10^{32} years, as predicted by early Grand Unified Theories [3, 4]. The most serious background for proton decay searches is atmospheric neutrino events, at a rate of approximately 10^2 events year^{-1} kt^{-1}.

Therefore, these experiments studied details of the observed atmospheric neutrino events [11, 12].

Current interest in the atmospheric neutrinos was initiated by the study of the ν_μ/ν_e flux ratio in the late 1980s [13]. The Kamiokande water Cherenkov experiment measured the number of e-like and μ-like events, which were mostly CC ν_e and ν_μ interactions, respectively. They found that the number of μ-like events had a significant deficit compared with the Monte Carlo prediction, while the number of e-like events had, in good agreement with the prediction [13]. The flavour ratio of the atmospheric neutrino flux, $(\nu_\mu + \bar{\nu}_\mu)/(\nu_e + \bar{\nu}_e)$, has been calculated to an accuracy of better than 5% in the relevant energy range. Because of the small $(\mu/\mathrm{e})_{\mathrm{Data}}/(\mu/\mathrm{e})_{\mathrm{Prediction}}$ ratio, it was concluded: 'We are unable to explain the data as the result of the systematic detector effects or uncertainties in the atmospheric neutrino fluxes. Some as-yet-accounted-for physics such as neutrino oscillations might explain the data'. This result triggered the interest in atmospheric neutrinos.[1] Consistent results were reported in the early 1990s from the IMB water Cherenkov experiment [14]. On the other hand, fine-grained iron calorimeter experiments, NUSEX [15] and Ferjus [16, 17], did not observe any significant ν_μ deficit within their statistics. Therefore, the situation was unclear in the early 1990s.

Another important hint towards the understanding of atmospheric neutrino phenomena was given in the mid-1990s [18]. Zenith angle distributions for multi-GeV fully-contained events and partially contained events were studied in Kamiokande. For detectors near the surface of the Earth, the neutrino flight distance, and thus the neutrino oscillation probability, is a function of the zenith angle of the neutrino direction. Vertically downward-going neutrinos travel about 15 km while vertically upward-going neutrinos travel about 13 000 km before interacting in the detector. The Kamiokande data showed that the deficit of μ-like events depended on the neutrino zenith angle. However, due to the relatively poor event statistics, the statistical significance of the up–down asymmetry in the Kamiokande data was 2.9 standard deviations and, therefore, the data were not conclusive. In 1998, the Super-Kamiokande experiment, with substantially larger data statistics than those in the previous experiments, concluded that the atmospheric neutrino data gave evidence for neutrinos oscillations [19]. Various detailed studies of neutrino oscillations have been made using atmospheric neutrino data. The atmospheric neutrino experiments are still contributing substantially to our understanding of neutrino masses and mixing angles.

In the following sections, details of the atmospheric neutrino observations are described. Section 2 describes the calculation of atmospheric neutrino fluxes. Section 3 outlines the simulation of neutrino interactions relevant to the energy range of atmospheric neutrinos. Sections 4 and 5 describe the details of the atmospheric neutrino data and the neutrino oscillation analyses. Then, in section 6, future prospects of the atmospheric neutrino experiments are briefly described. Section 7 summarizes the paper. In most of this paper, when mention is made of neutrinos, we imply both neutrinos and anti-neutrinos.

[1] We, however, note that a deficit of ν_μ events was already observed in the late 1970s [10]. The observed ν_μ flux in the South Africa experiment was only about 60% of that expected. This result is approximately consistent with data from the present experiments. However, due to the uncertainty in the predicted flux, no strong conclusion was made. Also, in 1986, IMB noticed that the observed fraction of events with electrons from muon decay was smaller than expected [11]. This can be explained by the deficit of CC ν_μ events. However, detailed study of the cause for the deficit was not made. A similar, but statistically less significant, effect was observed in Kamiokande (figure 19 of [12]) as well.

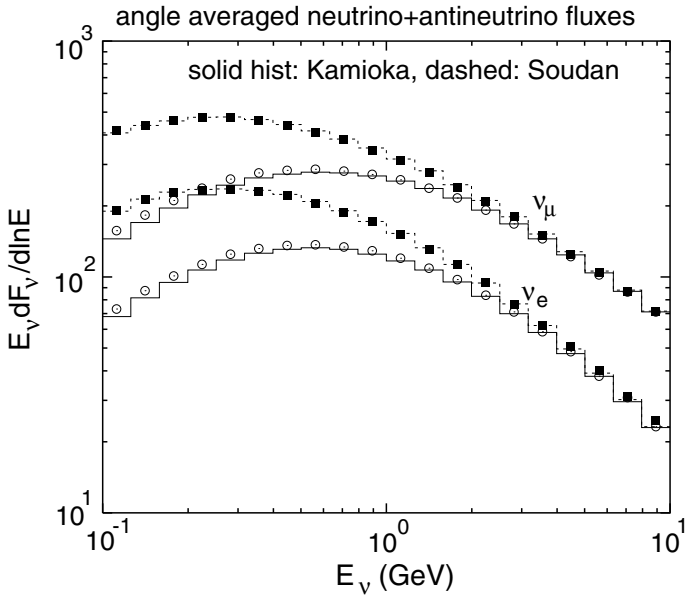

Figure 2. (a) The atmospheric neutrino energy spectrum calculated for the Kamioka and Soudan-2 sites [21]. The $(\nu_\mu + \bar{\nu}_\mu)$ and $(\nu_e + \bar{\nu}_e)$ fluxes are plotted for the three-dimensional (⊙) and one-dimensional (■) calculations. ——, histograms for Kamioka site and - - - -, histograms for the Soudan-2 site.

2. Atmospheric neutrino flux

To carry out detailed studies of neutrino oscillations using atmospheric neutrinos, it is important to know the expected flux in the absence of neutrino oscillations. The difficulties and uncertainties in the calculation of atmospheric neutrino fluxes differ between high and low energies. For low-energy neutrinos with energies of about 1 GeV, the primary fluxes of cosmic ray components are relatively well known. On the other hand, the low-energy cosmic ray fluxes of $\lesssim$10 GeV are modulated by solar activity, and affected by the geomagnetic field through a rigidity (momentum/charge) cutoff. The cutoff is lower near the poles and, therefore, the low energy flux is higher for detector locations near the poles than for those near the equator. For high-energy neutrinos with energies $\gtrsim$100 GeV, primary cosmic rays with energies $>$1000 GeV are relevant. At these energies, solar activity and the rigidity cutoff do not affect the cosmic rays, but details of the higher energy primary cosmic ray flux are not as well measured.

We outline the methods and results of the three most detailed atmospheric neutrino flux calculations [20]–[22]. More detailed description of the flux calculation can be found in [23]. Unlike older calculations [24, 25] in which the secondary particles were assumed to travel in the direction of the primary cosmic ray (one-dimensional calculations), in these calculations three-dimensional Monte Carlo methods were used. Also, primary cosmic ray flux data were used; solar modulation and geomagnetic field effects were taken into account; and the interaction of cosmic ray particles with the air nucleus, the propagation of the secondary particles in the air and the decay of them are simulated.

The calculated energy spectra of atmospheric neutrinos, by the one- and three-dimensional methods, at Kamioka (Japan) and the Soudan mine (USA) are shown in figure 2. The accuracy

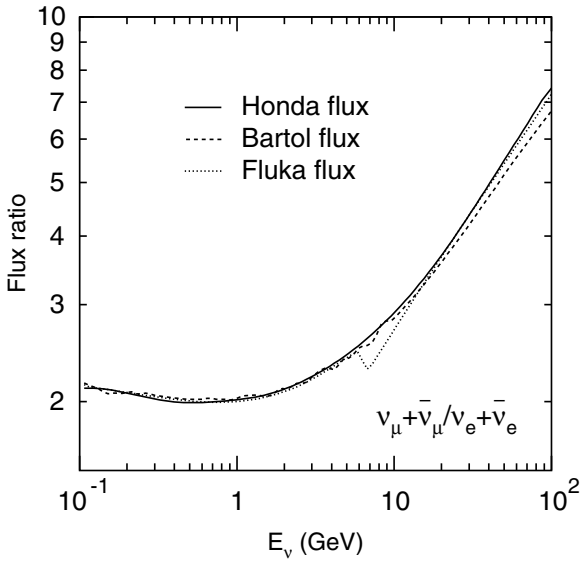

Figure 3. The flux ratio of $\nu_\mu + \overline{\nu}_\mu$ to $\nu_e + \overline{\nu}_e$ versus neutrino energy. Solid, broken and dotted lines show predictions of [20], [21] and [22], respectively.

in recent primary cosmic ray flux measurements [26, 27] below 100 GeV is about 5% and the data from independent experiments agree within the quoted uncertainties. However, the primary cosmic ray data are much less accurate above 100 GeV. Therefore, for neutrino energies $\lesssim$10 GeV, the calculated absolute flux should have a small uncertainty of about 10%. Indeed, calculated fluxes by [20], [21] and [22] agree within 10%. However, at much higher than 10 GeV, the uncertainties in the absolute neutrino flux must be substantially larger.

Figure 3 shows the calculated flux ratio of $\nu_\mu + \overline{\nu}_\mu$ to $\nu_e + \overline{\nu}_e$ as a function of the neutrino energy, integrated over solid angle. This ratio is essentially independent of the primary cosmic ray spectrum. The calculated flux ratio has a value of about 2 for energies less than a few GeV and increases with increase in neutrino energy. This is because a π-decay produces a ν_μ and a μ; the μ, when it decays, produces another ν_μ and a ν_e. Furthermore, three neutrinos produced in the chain decay of a π have approximately the same average energy. In the higher energy regions, the probability of a muon not to decay before reaching the ground increases with increase in muon energy. In the energy region of less than $\sim$10 GeV, most of the neutrinos are produced by the decay chain of pions and the expected uncertainty of this ratio is about 3%. In the higher energy region ($>$10 GeV), the contribution of K decay to the neutrino production is more important. There, the ratio depends more on the K production cross sections and the uncertainty of the ratio is expected to be larger.

Figure 4 shows the zenith angle dependence of the atmospheric neutrino fluxes for several neutrino energies and for two locations. At low energies and at the Kamioka location, the fluxes of downward-going neutrinos are lower than those of upward-going neutrinos. This is due to the cutoff of primary cosmic rays by the geomagnetic field. On the other hand, in North America, the fluxes of the downward-going neutrinos are higher than those of the upward-going neutrinos due to the very low rigidity cutoff. For neutrino energies higher than a few GeV, the calculated fluxes are essentially up–down symmetric, because the primary particles are more energetic than the rigidity cutoff. The enhancement of the flux near the horizon for low-energy neutrinos is a

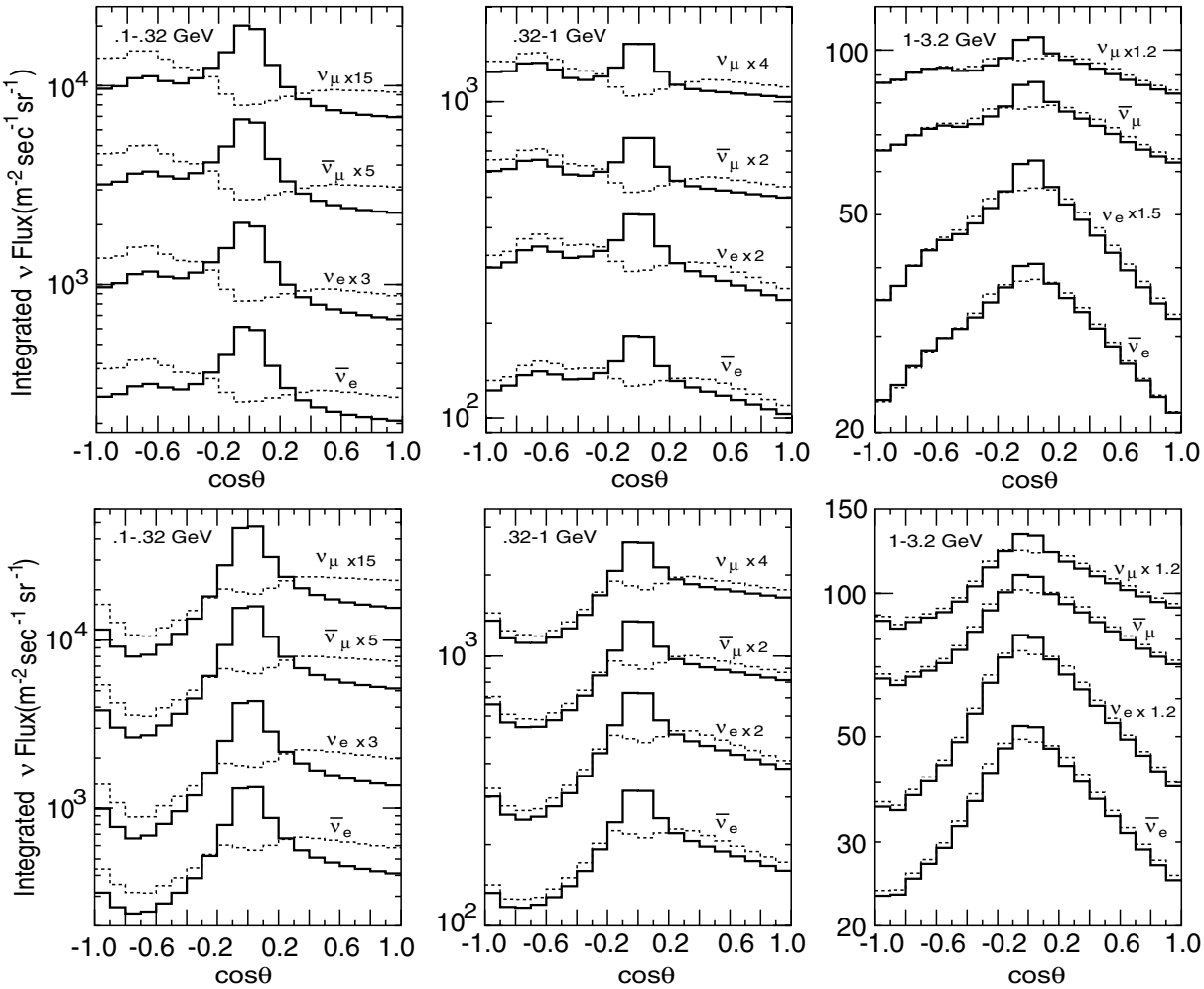

Figure 4. The flux of atmospheric neutrinos versus zenith angle for three neutrino energy ranges. Solid and broken lines show the prediction by three-dimensional and one-dimensional calculations [20], respectively. The upper panels are for the Kamioka site and the lower panels are for the North America sites (SNO and Soudan-2).

feature characteristic of full three-dimensional flux calculations, first reported in [22, 28] and confirmed by other calculations [20, 21]. The mechanism for the enhancement is discussed in [29]. The three-dimensional effect is only important below ∼1 GeV as seen in figure 4. However, the horizontal enhancement cannot be seen in the lepton zenith angle distribution, due to the relatively poor angular correlation between neutrinos and leptons below 1 GeV.

The uncertainties in the up–down and vertical–horizontal ratios of the number of events can be estimated by comparing the predicted ratios by various flux models. These uncertainties generally depend on the energy and the neutrino flavour. The uncertainty in the up–down event ratio is about 1–2% in the energy region below 1 GeV and is less than 1% above 1 GeV. The main source of the uncertainty in the vertical–horizontal ratio around a GeV is the size of the horizontal enhancement of the flux due to the three-dimensional effect; the uncertainty is estimated to be a few per cent. In the higher energy region, where upward through-going muons are relevant,

the largest source of the uncertainty in the vertical–horizontal ratio is the K production cross section, and the vertical–horizontal uncertainty is estimated to be 3% [30].

Summarizing the details of the atmospheric neutrino flux, we remark that, while the absolute flux value has a relatively large, energy-dependent uncertainty of about 10–30%, the $(\nu_\mu + \overline{\nu}_\mu/(\nu_e + \overline{\nu}_e)$ flux ratio is predicted to an accuracy of about 3%. The zenith-angle dependence of the flux is well understood, and especially, above a few GeV neutrino energies, the flux is predicted to be up–down symmetric.

3. Neutrino interactions

The important energy range for atmospheric neutrino interactions is between 0.1 GeV and 10 TeV. The Monte Carlo technique is used to simulate the neutrino interactions.

Usually, the following charged and neutral current (NC) neutrino interactions are considered in the simulation program.

- (quasi-)elastic scattering, $\nu\,\mathrm{N} \rightarrow \mathrm{l}\,\mathrm{N}'$,
- single-meson production, $\nu\,\mathrm{N} \rightarrow \mathrm{l}\,\mathrm{N}'\mathrm{m}$,
- coherent π production, $\nu\,{}^{16}\mathrm{O} \rightarrow \mathrm{l}\,\pi\,{}^{16}\mathrm{O}$,
- deep inelastic scattering, $\nu\,\mathrm{N} \rightarrow \mathrm{l}\,\mathrm{N}'$ hadrons.

Here, N and N′ are the nucleons (proton or neutron), l is the lepton and m is the meson, respectively. The most dominantly produced mesons are pions. If the neutrino interaction occurred in a nucleus, generated particles like pions and kaons interact with the nucleus before escaping from nuclei.

In the lowest energy range of <1 GeV, the quasi-elastic scattering [31] is dominant. For scattering off nucleons in ^{16}O, the Fermi motion of the nucleons and Pauli exclusion principle are taken into account. Usually, these effects are treated based on the relativistic Fermi gas model [32]. In the GeV energy range, the single-pion production processes [33, 34] are also important. In the multi-GeV or higher energy ranges, the deep inelastic scattering is dominant. Finally, it should be mentioned that high statistics neutrino interaction data taken by recent neutrino oscillation experiments are very important to improve the simulation of atmospheric neutrino interactions.

The total CC cross sections, together with the cross sections for quasi-elastic scattering, single meson productions and deep inelastic scattering, are shown in figure 5.

4. Atmospheric neutrino experiments

The rate of the atmospheric neutrino interactions is about $200\,\mathrm{kt}^{-1}\,\mathrm{year}^{-1}$. Since the background rate at the surface due to cosmic ray particles is very frequent, namely $\sim 2 \times 10^2\,\mathrm{m}^{-2}\,\mathrm{s}^{-1}$, it is unrealistic to carry out atmospheric neutrino experiments at the surface with the present technology. The hadrons, electrons and gammas still remaining at the surface are quickly absorbed by several metres of rock. Muons, consisting of a large fraction of the secondary cosmic rays at the surface, on the other hand, lose their energy only by ionization. If one wants to decrease the atmospheric muon flux significantly, the detector must be located deep underground.

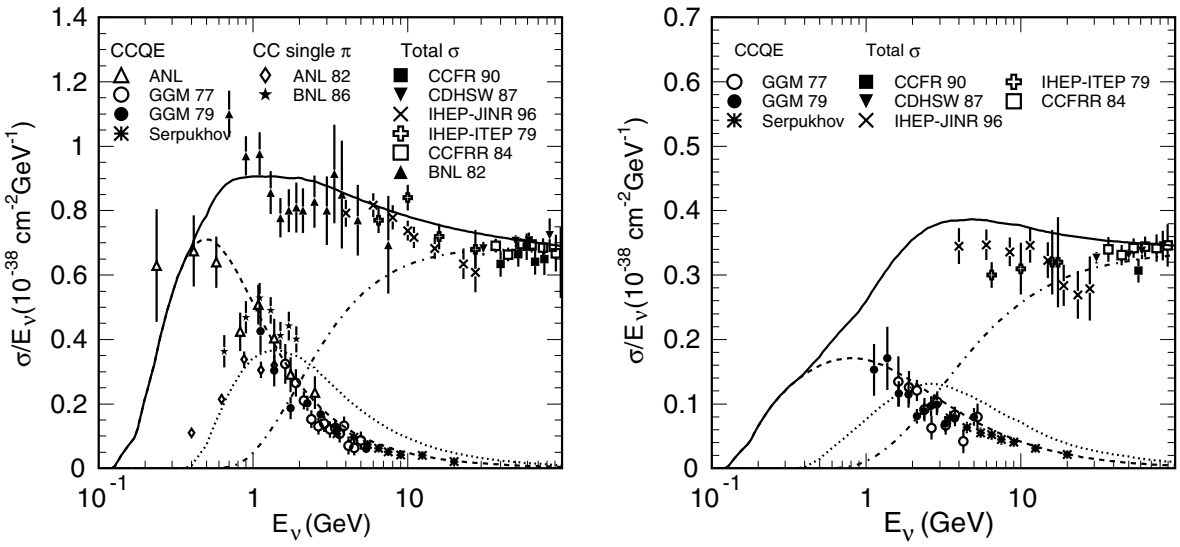

Figure 5. CC total cross section divided by E_ν for (a) neutrino and (b) anti-neutrino nucleon interactions. Solid lines show the calculated total cross sections. The broken, dotted and dash-dotted lines show the calculated quasi-elastic, single-meson and deep-inelastic scattering cross sections, respectively. Data points from various experiments are also shown. (The reference can be found in [44].)

Figure 6 shows the depth of the detectors and the cosmic ray muon rate. Even at a depth of 2700 m.w.e. (1000 m underground for the standard rock), Super-Kamiokande observes about two muons s^{-1}. This rate should be compared with the observed atmospheric neutrino rate in the fiducial volume of the same detector, about nine events day^{-1}. The rate of muons is $\sim 2 \times 10^4$ times more frequent than that of atmospheric neutrino events in Super-Kamiokande.

To date, two significantly different techniques, water Cherenkov detectors and fine-grained tracking detectors, have been used to observe atmospheric neutrino events. Each of these techniques will be described below.

4.1. Water Cherenkov detectors

In water Cherenkov detectors, an atmospheric neutrino event is detected by observing Cherenkov radiation from relativistic charged particles produced by the neutrino interaction with the nucleus. A two-dimensional array of photomultiplier tubes on the inside surface of the detector detects the photons. The hit time and the pulse height from each PMT are recorded. The timing information, with a typical resolution of a few nanoseconds for a single photoelectron pulse, is useful for reconstruction of the vertex position. The total number of photo-electrons gives information on the energy of the particles above the Cherenkov threshold. Figure 7 shows fully contained atmospheric neutrino events observed in the Super-Kamiokande detector.

The first-generation water Cherenkov detectors were IMB and Kamiokande. IMB [36] started taking data in 1982 and ended in 1991 after two major upgrades. The first phase of the detector (IMB-1) was equipped with 2048 PMTs each of 5-inch diameter. The light collection was improved by the addition of 2 feet × 2 feet × 0.5 inch wave-shifting plates, for a brief

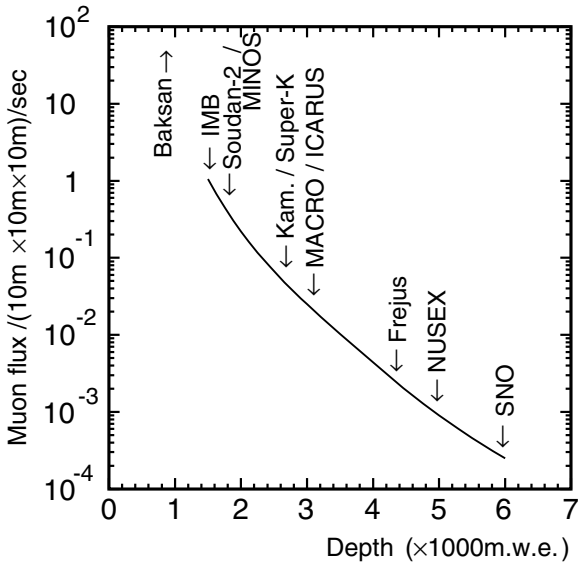

Figure 6. Depth of the detectors and the calculated cosmic ray muon rate (——). This figure is modified from [35].

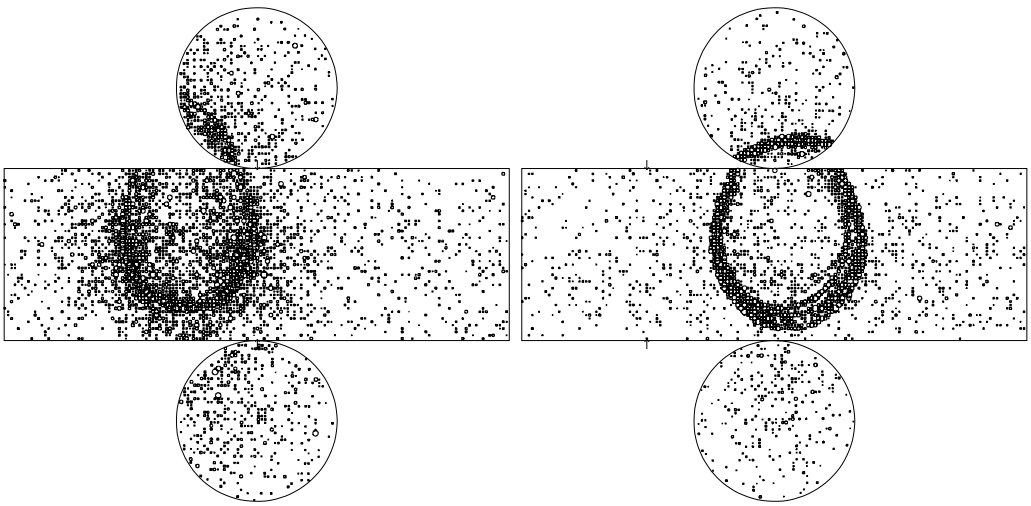

Figure 7. Example event displays from the Super-Kamiokande detector. Signals observed by the inner detector are shown. The left figure shows an electron event and the right one shows a muon event. The size of the circles shows the observed intensity of the photons by the PMTs that are installed at the position of the circles.

running period (IMB-2). Finally, the detector was equipped with 2048 8-inch PMTs, again with a wavelength shifter plate (IMB-3). It had a total mass and fiducial mass of 8 and 3.3 kt, respectively.

Kamiokande [37] started taking data in 1983 and ended in 1996. The Kamiokande detector used 1000 PMTs with 20-inch diameter, a photo cathode coverage of 20%. For the second phase, Kamiokande had an outer detector with thickness of the water between 0.5 and 1.5 m. The outer detector made it possible to identify the exiting atmospheric neutrino events (partially

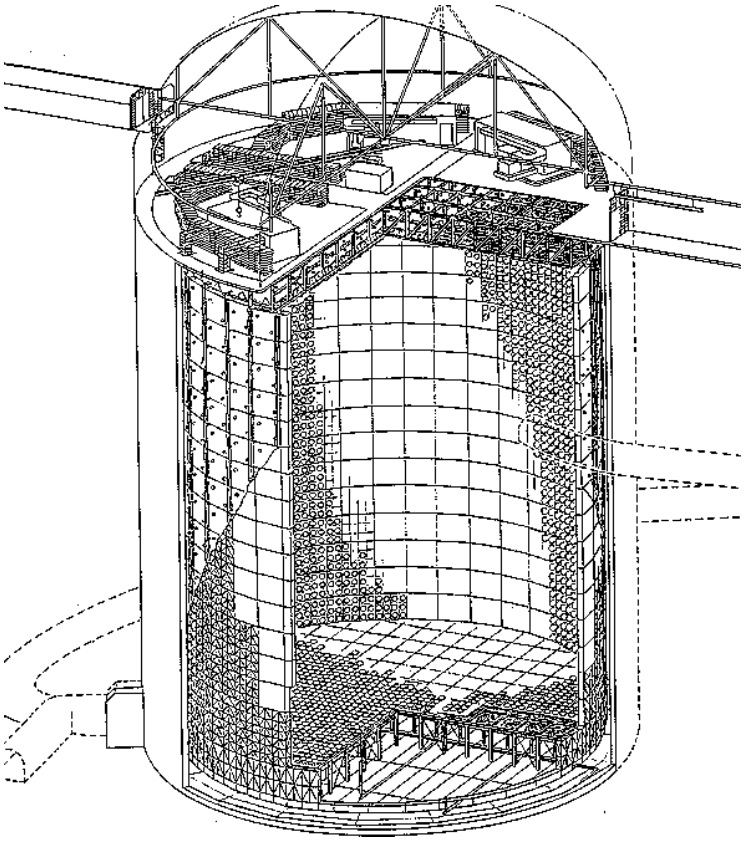

Figure 8. The Super-Kamiokande detector. It is a 50 kt water Cherenkov detector and is located 1000 m underground.

contained events) [18]. The detector was smaller than IMB: the total and fiducial masses were 4.5 and 1.04–1.35 kt, respectively. This detector showed that a water Cherenkov detector is able to separate electrons and muons very efficiently, thereby providing the possibility of studying neutrino oscillations using atmospheric neutrinos.

The present generation water Cherenkov detector is Super-Kamiokande [38] (see figure 8), whose results dominate our understanding of atmospheric neutrinos. It began taking data in 1996. It has a total mass of 50 kt. It uses 11 146 PMTs, each of 20-inch diameter with a photo-cathode coverage of 40% of the inner detector surface, a factor of two higher than that of Kamiokande. An outer detector surrounds the inner detector with 2 m thickness of water, equipped with 1885 8-inch PMTs with wavelength-shifting plates. The fiducial volume for neutrino vertices is 2 m from the plane of photomultiplier tubes, resulting in a 22.5 kt mass. The large mass and photocathode coverage allow for high statistics and detailed studies of atmospheric neutrinos.

4.2. Fine-grained tracking detectors

The second category of atmospheric neutrino detectors consists of comparatively fine resolution tracking detectors. The first generation of these experiments includes NUSEX [39] and Frejus [40]. These detectors were smaller than the water Cherenkov detectors in the 1980s. Tracking detectors have an advantage in sensitivity because they can detect low momentum charged

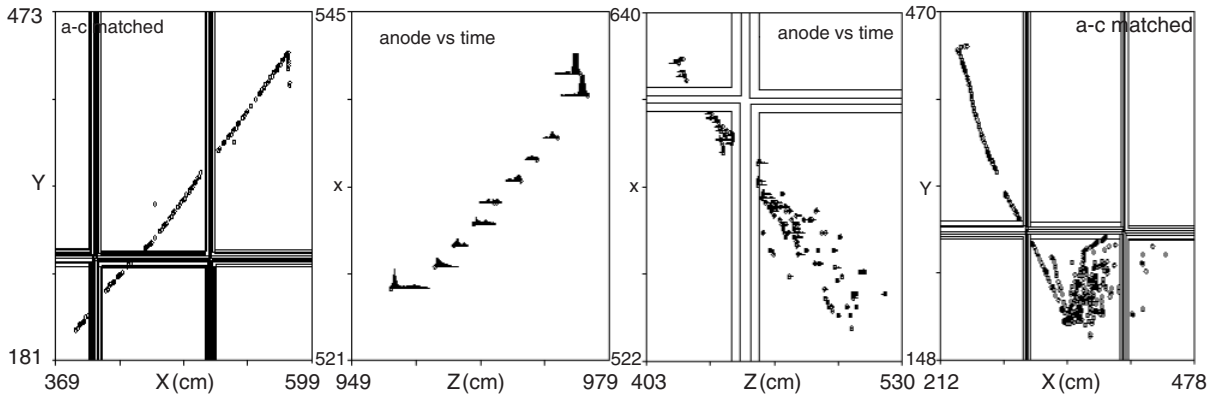

Figure 9. Example event displays from the Soudan-2 detector, showing the long track from a muon and a shorter, more heavily ionizing track from a recoil proton.

particles that would be below the Cherenkov threshold in water. In particular, the Soudan-2 detector [41] is able to reconstruct the short and heavily ionizing trajectory of recoil protons from atmospheric neutrino events such as $\nu n \rightarrow \mu p$, as shown in figure 9. The Soudan-2 detector is equipped with anti-counters. The anti-counter was useful to estimate the fraction of non-neutrino background events in the atmospheric neutrino sample as well as to eliminate cosmic ray background events easily.

There is a second type of fine-grained tracking detector that is mostly sensitive to muon neutrinos in the form of upward-going muons. These include the Baksan [42] and MACRO [43] experiments, which have fairly small absorber mass (a few hundred tons). These detectors identify the direction of the muon by resolving the time-of-flight as it traverses two or more layers of the liquid scintillator. The MACRO detector is composed of three horizontal planes with the lower section filled with crushed rock absorber and a hollow upper section. In addition to through-going muons, MACRO has analysed partially contained and stopping muon topologies, where the crushed rock in the lower section acts as neutrino target or muon stopper, respectively.

Table 1 summarizes major atmospheric neutrino detectors.

5. Observation of atmospheric neutrinos

5.1. Selection of atmospheric neutrino events

In very deep underground experiments such as Frejus [40] and NUSEX [39], the trigger rates were very low, about 7 and 45 events h^{-1} for NUSEX and Frejus, respectively. Hence, atmospheric neutrino events were simply selected by requiring the primary vertex in the fiducial volume.

Typically, detectors located at less deep places consisted of an outer anti-counter and an inner detector. In Kamiokande and Super-Kamiokande, most of the cosmic ray muons were rejected by requiring no signal in the anti-counter in selecting FC events. In Kamiokande, the remaining events were doubly scanned by physicists to select atmospheric neutrino events. In Super-Kamiokande, additional software cuts were applied to eliminate the remaining background events. The event scanning is not used to reject background events [44]. The selection of PC events is more complicated, because these events have anti-counter signals. However, even for

Table 1. Summary of the atmospheric neutrino experiments which observed fully contained (FC), partially contained (PC), upward-stopping muon and upward-through-going muon events.

Experiment	Detection technique	Type of events	Fiducial mass (kt)	Total exposure	Number of events
Baksan	Liquid scintillator	Up-through-μ	–	10.55 year	424
NUSEX	Gas counter-iron plate	FC	0.13	0.74 kt · year	50
Frejus	Gas counter-iron plate	FC	0.7	2.0 kt · year	158
		PC	0.7	2.0 kt · year	58
Kamiokande	Water Cherenkov	FC	1.04–1.35	7.7–8.2 kt · year	885
		PC	1.04	6.0 kt · year	118
		Up-through-μ	–	6.7 year	372
IMB	Water Cherenkov	FC	3.3	7.7 kt · year	935
		Up-through-μ	–	3.6 year	532
		Up-stopping-μ	–	3.6 year	85
Soudan-2	Gas counter-iron plate	FC	0.77	5.9 kt · year	379.5[a]
		PC		5.9 kt · year	57.7[a]
MACRO	Liquid scintillator + gas counter	Up-through-μ	–	6.17 year[b]	857[c]
			–	5.6 year	262[c]
			–	5.8 year	157[c]
Super-Kamiokande	Water Cherenkov	FC	22.5	92 kt · year	12180
		PC	22.5	92 kt · year	911
		Up-through-μ	–	4.5 year	1841.6[c]
		Up-stopping-μ	–	4.5 year	417.7[c]

[a] >300 MeV/c is required. Background events are statistically subtracted.
[b] Exposure with the partial detector configuration is normalized to the full detector configuration [45, 52].
[c] Background events are statistically subtracted.

these events, the information of the anti-counter is very useful. For example, by requiring only one anti-counter signal cluster, most of the cosmic ray muons are eliminated, because they typically produce two signal clusters at their entrance and exit points, while PC events typically have only one signal cluster. In Super-Kamiokande, various software cuts eliminate these background events and the event sample of PC events was selected without event scanning [44].

In Soudan-2, a different approach was taken. Events with reconstructed vertices in the fiducial volume were selected without using any anti-counter information. Then, the events were classified into 'quiet shield' and 'rock' events according to the anti-counter information. 'Quiet shield' events have no anti-counter hit signal and should be primarily neutrino events. The 'rock' events have anti-counter hits and are background events. Since there could be some contamination of background events among the 'quiet shield' events, the distribution of the minimum distance between the event vertex and the detector surface was studied. Generally, the vertex positions of the background events should cluster near the surface of the detector. About 90% of the 'quiet shield' events with the minimum momentum of 300 MeV/ c were fitted as neutrino events, and were used for further analyses.

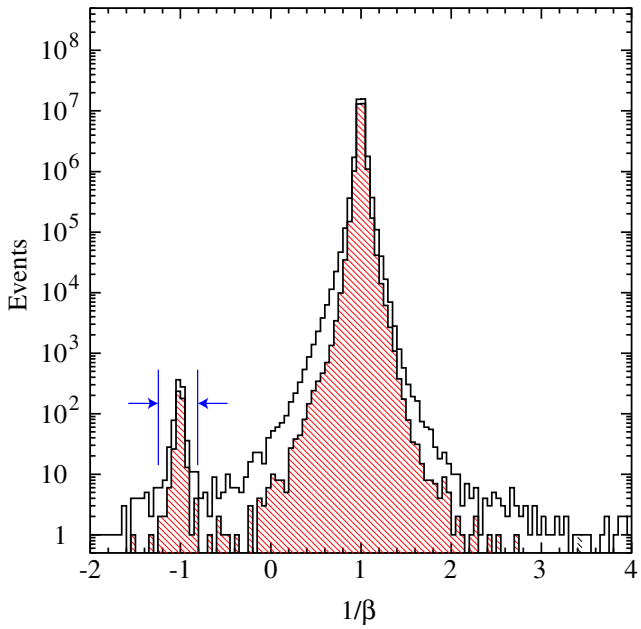

Figure 10. Reconstructed $1/\beta$ distribution for through-going particles observed in MACRO. $1/\beta = 1$ (-1) means downward-going (upward-going) particles with $\beta = 1$.

The selection of upward-going muons relies on a completely different algorithm. Typically, the track of every muon that enters the detector is reconstructed. Only muons that travel upward are selected. Figure 10 shows the reconstructed inverse velocity $(1/\beta)$ distribution for through-going particles observed in MACRO. Two clusters of events are seen near $1/\beta = -1$ and 1. They correspond to the downward-going muons $(1/\beta = 1)$ and upward-going muons $(1/\beta = -1)$. The contaminations of non-neutrino background events in the upward-going muon samples are generally small in the present generation atmospheric neutrino experiments. Estimated background contaminations range from $<1\%$ to several per cent, depending on the location of the detector and the category of events.

5.2. General features

Before discussing the data related to neutrino oscillations, we briefly discuss data statistics and some distributions that are relatively insensitive to neutrino oscillations.

The number of observed events and the detector exposures from each experiment are summarized in table 1.

The vertex positions of atmospheric neutrino interactions must be distributed uniformly within the detector. On the other hand, the vertex positions of background events should be clustered near the surface of the detector. The distribution of vertex positions is therefore an important check for background contamination. Figure 11 shows the distribution of the vertex position for fully contained events in Super-Kamiokande. The observed event rate was lower than that for the Monte Carlo prediction. We note that the Monte Carlo does not include neutrino oscillations. An excess of events near the walls of the inner detector is seen. However, this excess rapidly disappears as the vertex position moved to the inner region. Within the fiducial volume of 2 m from the inner detector walls, there is no evidence for background contamination.

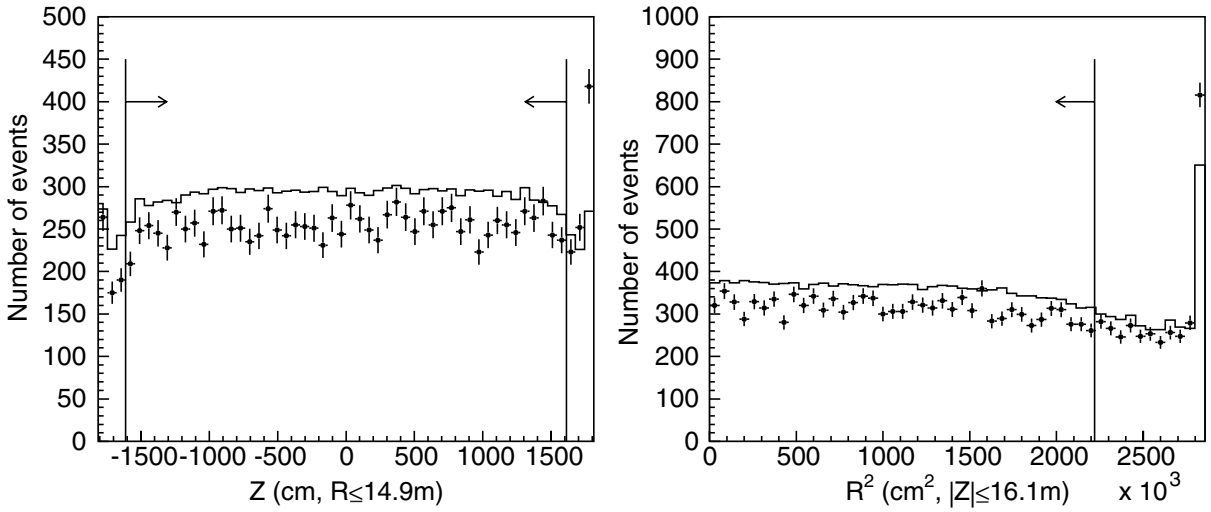

Figure 11. The distribution of fully contained event vertices in the vertical (left) and horizontal (right) coordinates, compared with the Super-Kamiokande data and atmospheric neutrino Monte Carlo prediction. The points show the data and the histogram shows the Monte Carlo prediction. Arrows indicate the fiducial region for the contained events. Neutrino oscillation is not included in the Monte Carlo calculation.

A similar study was carried out by the Soudan-2 experiment (see section 4). The background contamination in the Soudan-2 FC sample was estimated to be about 10%. The larger background contamination in Soudan-2 compared with Super-Kamiokande can be understood to be due to the shallower detector position and the thinner detector region outside of the fiducial volume in Soudan-2.

Figure 12 shows the momentum distribution for fully contained single-ring e-like and μ-like events observed in Super-Kamiokande. The shape of these distributions agreed well with the corresponding Monte Carlo predictions over a wide momentum range. The cutoff of the high-energy muon spectrum is due to the requirement of full-containment in the detector. A deficit of μ-like events in the whole momentum range is seen. This deficit is explained by neutrino oscillations.

In summary, the atmospheric neutrino data samples have, generally, high purity, and the Monte Carlo prediction reasonably reproduces the basic distributions of the data.

5.3. μ/e ratio

The atmospheric (ν_μ/ν_e) flux ratio has been measured by identifying electrons and muons produced by CC ν_e and CC ν_μ interactions, respectively. Electrons produce electromagnetic showers while propagating in matter. On the other hand, muons slowly lose their energy by $\mathrm{d}E/\mathrm{d}x$ while propagating in matter. The different propagation of these particles in matter is used to separate electrons and muons.

In tracking calorimeters, the event pattern is recorded in a three-dimensional view, and the separation of electrons and muons is carried out by event pattern recognition. Figure 9 shows examples of events observed by the Soudan-2 detector. CC ν_μ events are clearly recognized

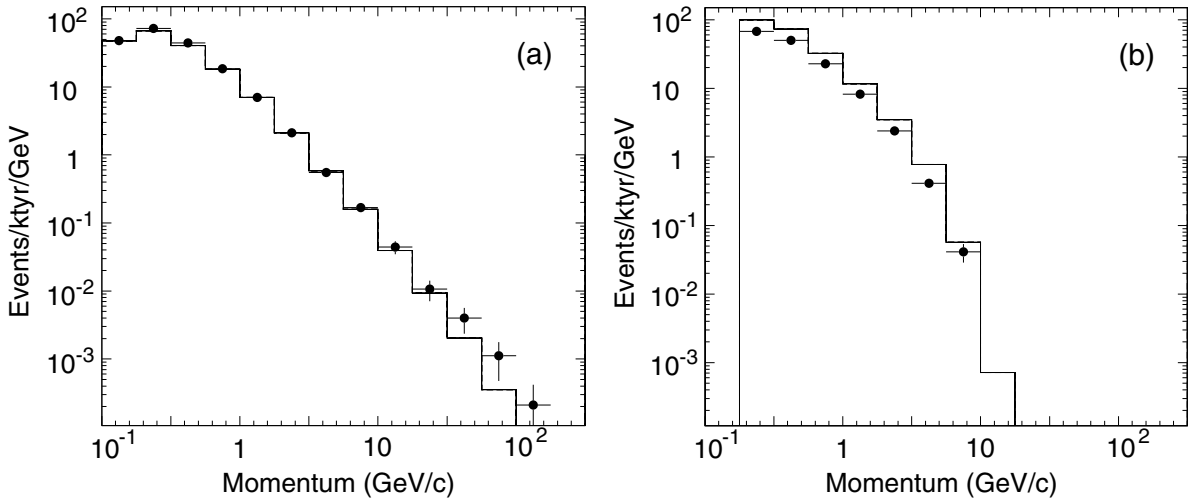

Figure 12. Momentum distributions for fully-contained single-ring (a) e-like and (b) μ-like events observed in Super-Kamiokande during 92 kt · year exposure of the detector. The Monte Carlo prediction does not include neutrino oscillations.

by a long straight track, which is a candidate muon. A CC ν_e event, on the other hand, has an electromagnetic shower linked to the vertex point.

In water Cherenkov detectors, CC ν_e and CC ν_μ events are distinguished by the difference in the characteristic shape of the Cherenkov ring. Figure 7 shows an e-like and a μ-like event observed in the Super-Kamiokande detector. A clear outer edge of the Cherenkov light is identified for a μ-like event, while the edge is relatively unclear for an e-like event due to an electromagnetic shower and the multiple scattering of low-energy electrons.

On the basis of the particle identification technique, the flavour ratio in the atmospheric neutrino flux was measured. The $(\nu_\mu + \overline{\nu}_\mu)/(\nu_e + \overline{\nu}_e)$ flux ratio has been calculated to an accuracy of about 3%, and therefore the measurement of this ratio is sensitive to neutrino oscillations. Experimentally, the μ-like/e-like ratio for the data is compared with that for the MC. Therefore, $(\mu\text{-like/e-like})_{\text{Data}}/(\mu\text{-like/e-like})_{\text{MC}}$ should be consistent with unity within the errors for the case of no neutrino oscillations. Figure 13 summarizes the $(\mu/\text{e})_{\text{Data}}/(\mu/\text{e})_{\text{MC}}$ measurements from various experiments. Measurements from Kamiokande (both sub- and multi-GeV data samples) [18, 46], IMB-3 (sub-GeV) [14], Soudan-2 [47] and Super-Kamiokande [19, 44] (both sub- and multi-GeV data samples) showed $(\mu/\text{e})_{\text{Data}}/(\mu/\text{e})_{\text{MC}}$ ratios which were smaller than unity. The sub-GeV (multi-GeV) sample in Kamiokande and Super-Kamiokande was defined to include events with $E_{\text{vis}} < 1.33$ (>1.33) GeV, where E_{vis} is the visible energy. $E_{\text{vis}} = 1.33$ GeV corresponds to an electron (muon) momentum of 1.33 (about 1.4) GeV/c. There were a few measurements [15, 17, 48] suggesting a ratio consistent with unity. However, these measurements had relatively large statistical errors.

Since many of the uncertainties of the prediction and the experiment cancel when taking this ratio, the systematic error of this measurement was relatively small. Neither a statistical fluctuation nor systematic uncertainties can explain the small (μ/e) ratio of the data.

The small μ/e ratio could be interpreted as due to neutrino oscillations between $\nu_\mu \leftrightarrow \nu_\tau$ or $\nu_\mu \leftrightarrow \nu_e$ with a large mixing angle. However, there were other possibilities that could explain the data. For example, Mann *et al* [49] suggested that the data could be explained by proton decay

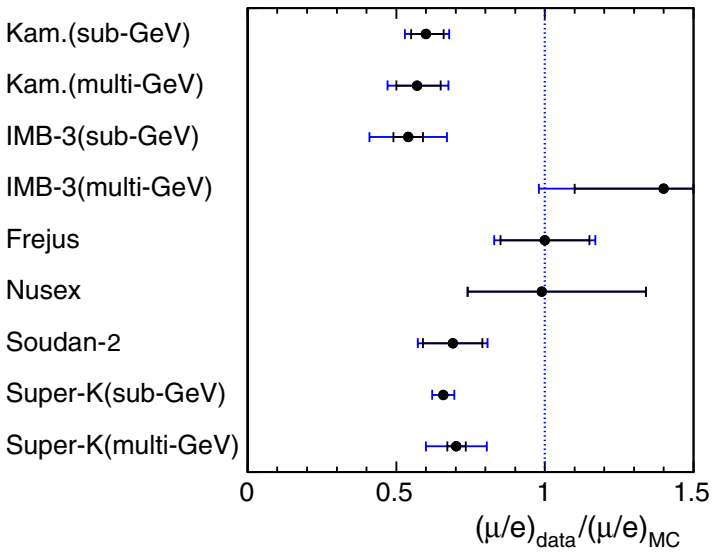

Figure 13. Summary of the measurements of the double ratio μ-like/e-like (data) to μ-like/e-like (Monte Carlo) by various atmospheric neutrino experiments. The inner and outer error bars show the statistical and statistical + systematic errors, respectively.

into $e^+\nu\nu$, since the observed small μ/e ratio could be interpreted as due to an excess of e-like signal by these positrons.

5.4. Zenith angle distribution

The atmospheric neutrino flux is predicted to be up–down symmetric above a few GeV neutrino energies. For downward-going neutrinos, the flight length is about 15 km, while that for vertically upward-going neutrinos it is 13 000 km. Therefore, if the neutrino oscillation length is O(100–1000 km), it should be possible to observe up–down asymmetry of the flux while the prediction is up–down symmetric. Early data from Kamiokande [18] showed that the upward-going multi-GeV μ-like events had substantially lower event rate than the downward-going ones, while an approximate up–down symmetry was expected.

The zenith angle distributions for e-like and μ-like events observed in Super-Kamiokande (92 kt · year) are shown in figure 14 [44, 50]. The μ-like data have exhibited a strong deficit of upward-going events, while no significant deficit has been observed in the e-like data. For further discussion, we define the up–down ratio U/D, where U is the number of upward-going events ($-1 < \cos\Theta < -0.2$, where Θ is the zenith angle) and D is the number of downward-going events ($0.2 < \cos\Theta < 1$). The ratio is expected to be near unity independent of flux model for $E_\nu > 1$ GeV, above which effects due to the Earth's magnetic field on cosmic rays are small. The U/D value for the multi-GeV FC + PC μ-like events from Super-Kamiokande, $0.55^{+0.035}_{-0.033}$(stat.) ± 0.005 (syst.) deviates from unity by 10 standard deviation (SD). Many systematic errors are cancelled for the U/D ratio. Hence the estimated systematic error in the U/D ratio is about 1% [44]. The observed up–down ratio suggests a near maximal neutrino mixing, because U/D can be approximately expressed as $U/D = 1 - \sin^2 2\theta_{23}/2$. For sub-GeV μ-like events, the observed ratio is larger than that in the multi-GeV sample due to the poorer angular resolution. Below 400 MeV c, the ratio is close to unity due to the very poor angular resolution.

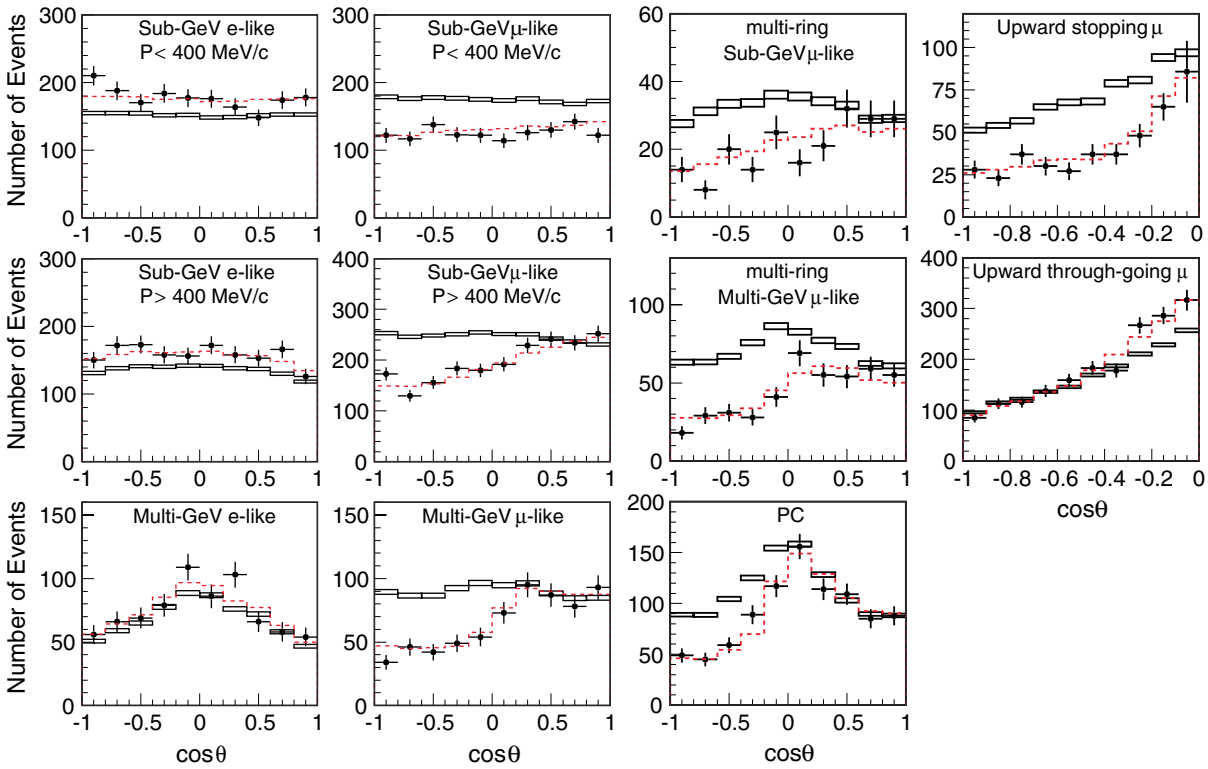

Figure 14. Zenith-angle distributions observed in Super-Kamiokande based on 92 kt · year data for various data samples; $\cos\Theta = 1\,(-1)$ corresponds to down-going (up-going). The solid line histograms show the prediction without neutrino oscillations. The broken line histograms show the prediction with $\nu_\mu \rightarrow \nu_\tau$ oscillations ($\Delta m^2_{23} = 2.1 \times 10^{-3}\,\mathrm{eV}^2$, $\sin^2 2\theta_{23} = 1.0$). In the oscillation prediction, various uncertainty parameters such as the absolute normalization were adjusted to give the best fit to the data.

The observed number of events for upward through-going muons was slightly higher than the no-oscillation prediction. We note that the predicted neutrino flux has more than 20% uncertainty in the energy range of >100 GeV. The observed zenith angle distribution is explained well by neutrino oscillations, if the large systematic uncertainty in the absolute flux is taken into account.

Figure 15 shows the zenith angle distributions observed in Soudan-2 (5.9 kt · year) [51]. Due to the geomagnetic field effect and the zenith angle-dependent detection efficiency for PC events, more downward-going events are predicted than the upward-going ones even for the no-oscillation case. Although the statistics of the Soudan-2 data are limited, the observed deficit of upward-going μ-like events is consistent with the Super-Kamiokande data.

Figure 16 shows the zenith angle distributions for three data samples observed in MACRO [52, 53]. The predicted and observed numbers of events near the horizon are small (or the error bars are large if the efficiency is corrected to estimate the flux in figure 16 (left panel)) due to the lower efficiency for near-horizontal events. The zenith angle distribution for upward-going PC events (figure 16, middle panel) shows a relatively large deficit of the data events, while that for upward-going stopping μ plus downward-going PC events shows only a small deficit

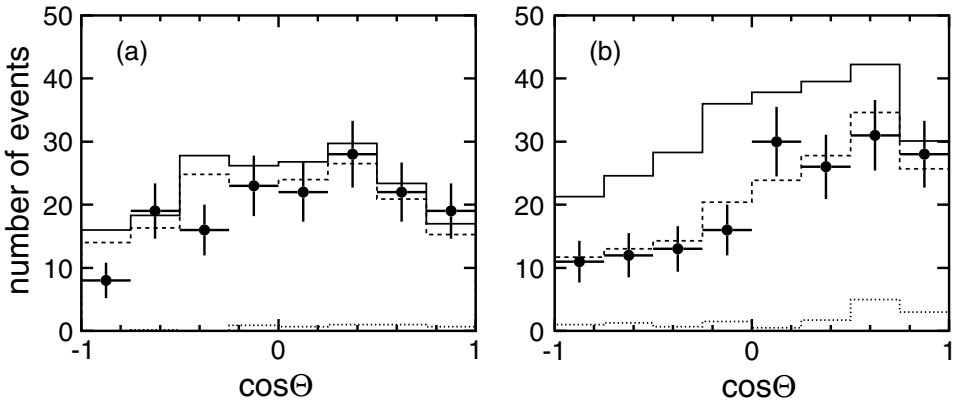

Figure 15. Zenith-angle distributions observed in Soudan-2 based on 5.9 kt · year data for the (a) CC ν_e and (b) CC ν_μ samples. The solid, broken and dotted line histograms show the Monte Carlo prediction without neutrino oscillations, with neutrino oscillations and the estimated background events, respectively.

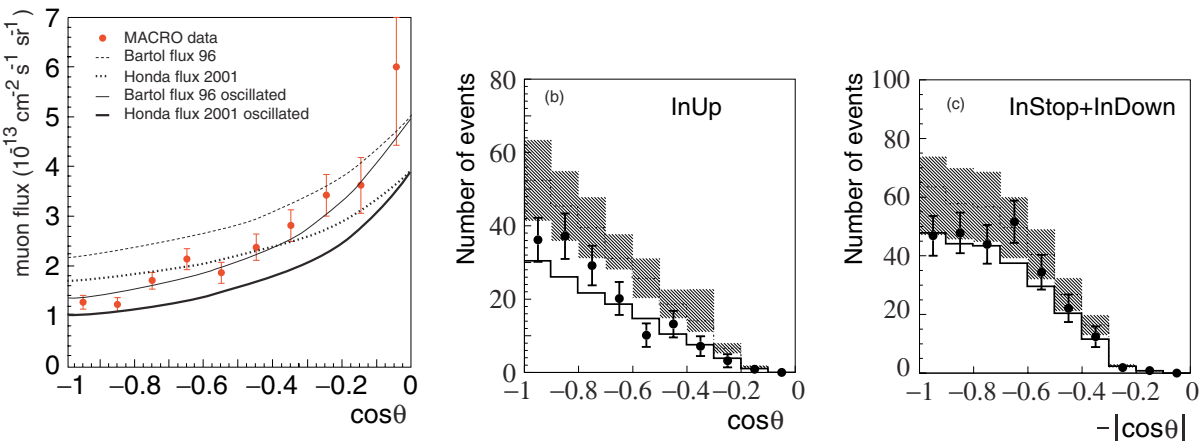

Figure 16. Zenith-angle distributions for the upward through-going muon flux (left), upward PC events (middle), and upward stopping muons plus downward PC events (right) observed in MACRO. For the middle and right panels, the lines with the shaded regions show the expectation for null oscillations with the absolute normalization uncertainty. The flux model used in the middle and right panels [22] gives a very similar flux prediction as the lower flux model in the left figure for upward-through-going muons. The solid lines show the expected flux for $\nu_\mu \to \nu_\tau$ oscillations with $(\sin^2 2\theta_{23} = 1.0,\ \Delta m^2_{23} = 2.3 \times 10^{-3}\,\mathrm{eV}^2)$.

of the data events. This can be understood by neutrino oscillations, since about a half of the upward-going neutrinos should be oscillated away, while the downward-going neutrinos have very little oscillation effects, and since the number of downward-going PC events and the number of upward-going stopping muon events are expected to be approximately equal for no oscillation. The MACRO data are also consistent with neutrino oscillations.

5.5. Two-flavour neutrino oscillation analysis

Since μ-like events show the zenith-angle- and energy-dependent deficit of events, while e-like events show no evidence for inconsistency between the data and non-oscillated Monte Carlo, it can be concluded that the oscillation could be between ν_μ and ν_τ. Indeed, detailed oscillation analyses of the Super-Kamiokande data [19, 44] have concluded that the data are consistent with two-flavour $\nu_\mu \to \nu_\tau$ oscillations. In the analysis of the atmospheric neutrino data, χ^2 methods that take into account various systematic uncertainties are typically used. For example, in the analysis of the Super-Kamiokande data, the χ^2 is defined to be

$$\chi^2 = \sum_{i=1}^{180} \frac{(N_i^{\rm obs} - N_i^{\rm exp})^2}{\sigma_i^2} + \sum_{j=1}^{37} \left(\frac{\epsilon_j}{\sigma_j}\right)^2. \tag{4}$$

Events are divided into 180 bins based on the event type, momentum and zenith angle. In the first sum, $N_i^{\rm obs}$ is the number of observed events in the ith bin and $N_i^{\rm exp}$ is the expected number of events based on a Monte Carlo simulation and σ_i combines the statistical uncertainties in the data and Monte Carlo simulation. During the fit, the values of $N_i^{\rm exp}$ are recalculated to account for neutrino oscillations, and systematic variations in the predicted rates due to uncertainties in the neutrino flux model, neutrino cross-section model and detector response. The second sum in the χ^2 definition takes into account the contributions from 37 variables which parametrized the systematic uncertainties in the expected neutrino rates. σ_j represents the systematic error for the jth term. The absolute normalization is treated as a free parameter, and does not contribute to the second term in the χ^2 definition. During the fit, these parameters are varied to minimize χ^2 for each choice of the oscillation parameters $\sin^2 2\theta$ and Δm^2. (See [54] for a description of the mathematical details.)

The estimated oscillation parameters ($\sin^2 2\theta$, Δm^2) for two-flavour $\nu_\mu \to \nu_\tau$ oscillations from various experiments [44, 51, 52, 55] are shown in figure 17. All results are essentially consistent. If the most accurate result from Super-Kamiokande is referred, the oscillation parameters are determined to be $\sin^2 2\theta > 0.92$ and $1.5 \times 10^{-3} < \Delta m^2 < 3.4 \times 10^{-3}\,{\rm eV}^2$ at 90% CL. Finally, we remark that consistent results have been obtained by a recent long-baseline neutrino oscillation experiment based on a neutrino beam produced by a proton accelerator [56, 57].

5.6. L/E analysis

The deficit of ν_μ events observed by the atmospheric neutrino experiments is explained very well by neutrino oscillations. However, there are models that explain the zenith angle- and energy-dependent deficit of ν_μ events reasonably well. They are neutrino decay [58] and neutrino decoherence [59, 60] models. These models may not be particularly appealing theoretically. However, it is still important to experimentally determine which is the right explanation for the atmospheric ν_μ deficit. One of the key features of neutrino oscillations is the sinusoidal ν_μ disappearance probability as a function of L/E. On the other hand, the ν_μ survival probability for the neutrino decay and decoherence models are not sinusoidal. Therefore, in order to further confirm neutrino oscillations, it is important to measure the sinusoidal neutrino oscillation feature.

Soudan-2 [51] and MACRO [61] analysed their data in terms of L/E. Results from these analyses are shown in figure 18. Because of the limited L/E resolution, these experiments were

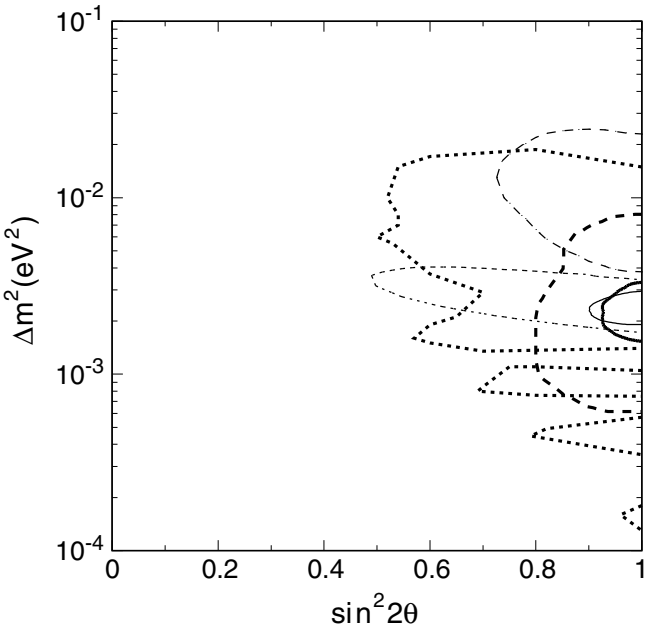

Figure 17. 90% C L allowed parameter regions of oscillation parameters from Super-Kamiokande (thick line), Kamiokande (thin broken line), Soudan-2 (thick dotted line) and MACRO (thick broken line). Two-flavour $\nu_\mu \rightarrow \nu_\tau$ oscillations are assumed. Also shown are the allowed regions from the L/E analysis in Super-Kamiokande (thin line) and the region obtained by the long-baseline experiment K2K (thin dotted line).

unable to see the first oscillation maximum (dip) that corresponds to $(1.27\Delta m^2 L)/E_\nu = \pi/2$. (Observing the second and the higher oscillation maxima is even more difficult, since an even better L/E resolution is required to observe these dips.)

Recently, Super-Kamiokande published an L/E analysis [62]. High L/E resolution events, which have an (L/E) resolution better than 70%, were used. Since L/E resolution depends on the zenith angle, energy and type of events, the events were selected using this information. Essentially, low-energy events are not used, because of the poor correlation between the neutrino and outgoing particles. Also, horizontal-going events are not used, because L changes significantly with a small change in the zenith angle near horizon. 2121 FC μ-like and 605 PC events were selected. Figure 19 (left panel) shows the number of events as a function of the reconstructed L/E, together with the MC prediction. Two clusters of events are visible below and above $150\,\mathrm{km\,GeV^{-1}}$. They mostly correspond to downward- and upward-going events, respectively.

Figure 19 (right panel) shows the ratio of the data over non-oscillated MC as a function of L/E together with the best-fit expectation for two-flavour $\nu_\mu \leftrightarrow \nu_\tau$ oscillations with systematic errors. A dip, which should correspond to the first maximum oscillation, is observed around $L/E = 500\,\mathrm{km\,GeV^{-1}}$. Due to the L/E resolution of the detector, the second and higher maximum oscillation points should not be observable in the Super-Kamiokande experiment. The data points at large L/E in figure 19 (right panel) show a slight deviation from the expected flat distribution. The Super-Kamiokande experiment concluded that the energy-dependent systematic effects such as the neutrino interaction cross sections are the main sources of non-flatness.

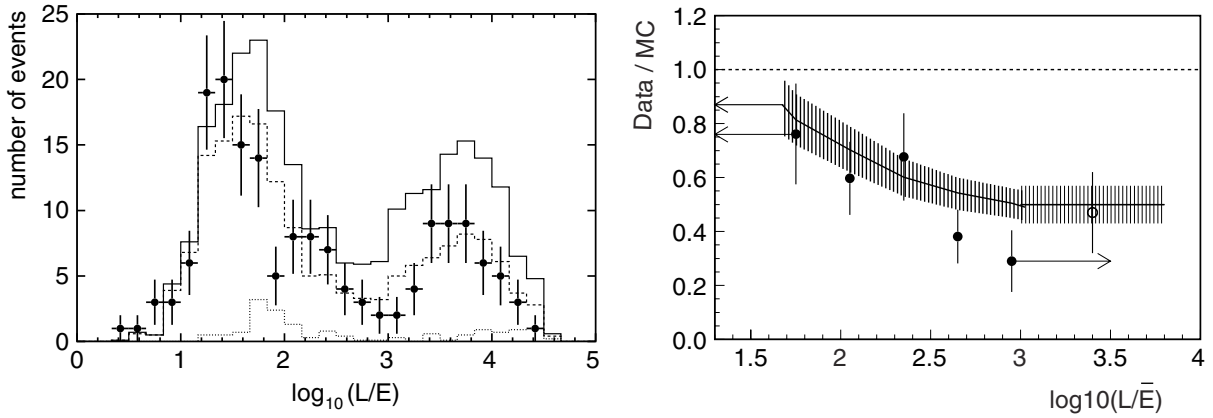

Figure 18. Left: number of μ-like events as a function of L/E for the Soudan-2 data (points) and the atmospheric neutrino MC events with and without oscillations (broken line and solid line histograms, respectively). Only high-resolution events are used. The estimated non-neutrino background events are also shown by the dotted line histogram. Right: ν_μ survival probability as a function of L/E obtained by analysis of the MACRO upward through-going muon data. The muon momentum is estimated from the multiple scattering. The expected distribution for oscillation is shown by the shaded line. The rightmost data point shows the result for upward-going PC events.

In the neutrino decay and decoherence models, it is assumed that a neutrino flavour eigenstate is a mixture of mass eigenstates. However, the mechanisms for generating ν_μ disappearance are different. In particular, these models do not predict sinusoidal ν_μ disappearance probability. Also shown in figure 19 are the L/E distributions for the best-fit expectation for the neutrino decay and decoherence models. Since these models cannot predict the dip observed in the data, the χ^2 values for these models were worse. The neutrino decay and decoherence models were disfavoured at 3.4 and 3.8 SD levels, respectively. The observed L/E distribution gives evidence that the neutrino flavour transition probability obeys a sinusoidal function as predicted by neutrino flavour oscillations.

The observed L/E distribution was used to estimate the $\nu_\mu \to \nu_\tau$ oscillation parameters. The definition for χ^2 was similar to that in equation (4). Figure 20 shows the contour plot of the allowed oscillation parameter regions. The 90% CL allowed parameter region was obtained as $1.9 \times 10^{-3}\,\mathrm{eV}^2 < \Delta m^2 < 3.0 \times 10^{-3}\,\mathrm{eV}^2$ and $\sin^2 2\theta > 0.90$. The result is consistent with that of the oscillation analysis using zenith-angle distributions (see figure 17).

5.7. Three-flavour neutrino oscillation analysis

As an extension of the two-flavour oscillation analysis, we discuss three-flavour neutrino oscillations. We assume that Δm^2_{12} is much smaller than $\Delta m^2_{23}(\Delta m^2_{13})$ as measured by solar neutrino [63, 64] and KamLAND experiments [65], and therefore assume the effect of the oscillations related to Δm^2_{12} is negligible in atmospheric neutrino experiments. The oscillation length relevant to Δm^2_{12} is shorter than the diameter of the earth for E_ν below 1 GeV. However, due to the accidental feature that the atmospheric ν_μ/ν_e ratio is ~ 2 in the absence of $\nu_\mu \to \nu_\tau$

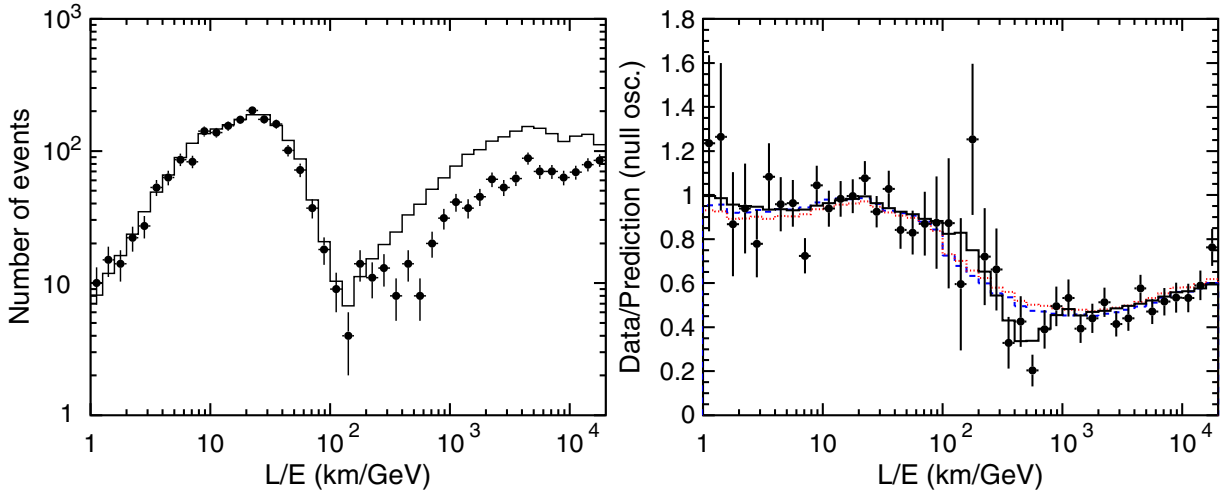

Figure 19. Left: number of events as a function of L/E for the Super-Kamiokande data (points) and the atmospheric neutrino MC events without oscillations (solid line histogram). The MC is normalized by the detector life-time. Right: ratio of the data to the MC events without neutrino oscillation (points) as a function of the reconstructed L/E together with the best-fit expectation for 2-flavour $\nu_\mu \leftrightarrow \nu_\tau$ oscillations (solid line). Also shown are the best-fit expectation for neutrino decay (dashed line) and neutrino decoherence (dotted line).

oscillations in the relevant energy range and the (near) maximal θ_{23} mixing angle, the effect of the oscillations related to Δm^2_{12} is predicted to be small [66, 67]. Under this approximation, there are only three oscillation parameters; θ_{13}, θ_{23} and Δm^2 ($\equiv \Delta m^2_{13} = \Delta m^2_{23}$). The neutrino oscillation probability in the vacuum can be written as

$$P(\nu_e \to \nu_e) = 1 - s^2 2\theta_{13} s^2 \left(\frac{1.27 \Delta m^2_{23}(\mathrm{eV}^2) L(\mathrm{km})}{E_\nu(\mathrm{GeV})} \right), \tag{5}$$

$$P(\nu_\mu \to \nu_e) = s^2\theta_{23} s^2 2\theta_{13} s^2 \left(\frac{1.27 \Delta m^2_{23} L}{E_\nu} \right), \tag{6}$$

$$P(\nu_\mu \to \nu_\mu) = 1 - 4c^2\theta_{13} s^2\theta_{23}(1 - c^2\theta_{13} s^2\theta_{23}) s^2 \left(\frac{1.27 \Delta m^2_{23} L}{E_\nu} \right), \tag{7}$$

where s and c represent sine and cosine, respectively. For $\theta_{13} = 0$, the oscillation is identical to two-flavour $\nu_\mu \to \nu_\tau$ oscillations. Only θ_{13} is the new parameter, and it represents the first- and third-generation neutrino mixing. Since ν_e is involved in the oscillation, the matter effect [68, 69] must be taken into account. The oscillation probability in the matter is different from that in vacuum for oscillations involving ν_e. This is due to the difference in the forward scattering amplitude for ν_e and ν_μ (or ν_τ). Assuming $\Delta m^3_{23} > 0$, the instantaneous mixing parameter ($\sin^2 2\theta^m_{13}$) in matter for neutrinos with the electron number density N_e is

$$\sin^2 2\theta^m_{13} = \frac{\sin^2 2\theta_{13}}{(A/\Delta m^2_{23} - \cos 2\theta_{13})^2 + \sin^2 2\theta_{13}}, \tag{8}$$

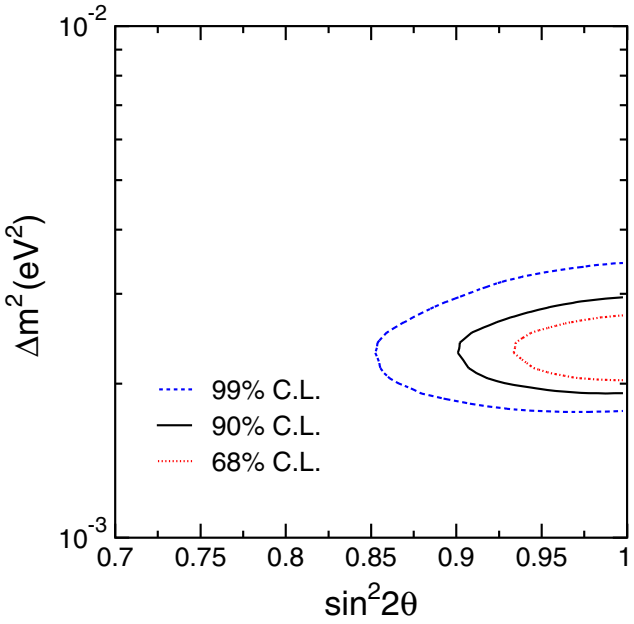

Figure 20. Oscillation parameter regions with 68, 90 and 99% allowed CL for two-flavour $\nu_\mu \leftrightarrow \nu_\tau$ oscillations obtained by the L/E analysis.

where $A = 2\sqrt{2}G_F N_e E_\nu$ (G_F is the Fermi coupling constant). For anti-neutrinos, A must be replaced by $-A$. If a condition $A = \Delta m^2 \cos 2\theta_{13}$ is satisfied, $\sin^2 2\theta_{13}^m$ is maximum (=1) even though the mixing angle θ_{13} is small. See, for example, [70, 71] for more complete discussions. For $\Delta m^2_{23} = 2$ to 3×10^{-3} eV^2 with a small θ_{13}, the resonance could occur for neutrinos passing through the Earth with their energies between 5 and 10 GeV. Therefore, the effect of a non-zero θ_{13} could be observed as an excess of electron neutrinos in the upward-going direction. Figure 21 (left) shows the $\nu_e \leftrightarrow \nu_\mu$ oscillation probability as a function of the neutrino energy and zenith angle. A clear resonance effect is seen for upward-going neutrinos near 5 GeV. For neutrinos passing through the core of the Earth, resonances will occur in slightly lower neutrino energies. This effect can be observed as an excess of upward going e-like events. Figure 21 (right) shows the expected excess e-like events in Super-Kamiokande for a set of oscillation parameters.

The present data from Super-Kamiokande (figure 14) and Soudan-2 (figure 15) show no evidence for an excess of e-like events in the upward-going direction. The preliminary result on allowed region of the oscillation parameters on the $\sin^2\theta_{13}$ and $\sin^2\theta_{23}$ plane is shown in figure 22 (left). In this analysis, data from Super-Kamiokande were used. Since the matter resonance effect occurs only for neutrinos (anti-neutrinos) if $m_3^2 - m_2^2 \equiv \Delta m^2_{23} > 0$ (<0), and since the sign of Δm^2_{23} is not known, the allowed regions were estimated for both positive and negative Δm^2_{23} cases. No evidence for non-zero $\sin^2\theta_{13}$ has been observed. The constraints on θ_{13} from reactor experiments [72, 73] are still more stringent than that from the atmospheric neutrino results, as seen in figure 22 (right).

5.8. Search for CC ν_τ events

If $\nu_\mu \rightarrow \nu_\tau$ is the dominant oscillation channel, about one CC ν_τ event per kt · year exposure can be expected to occur in an atmospheric neutrino detector. The low event rate is due to the

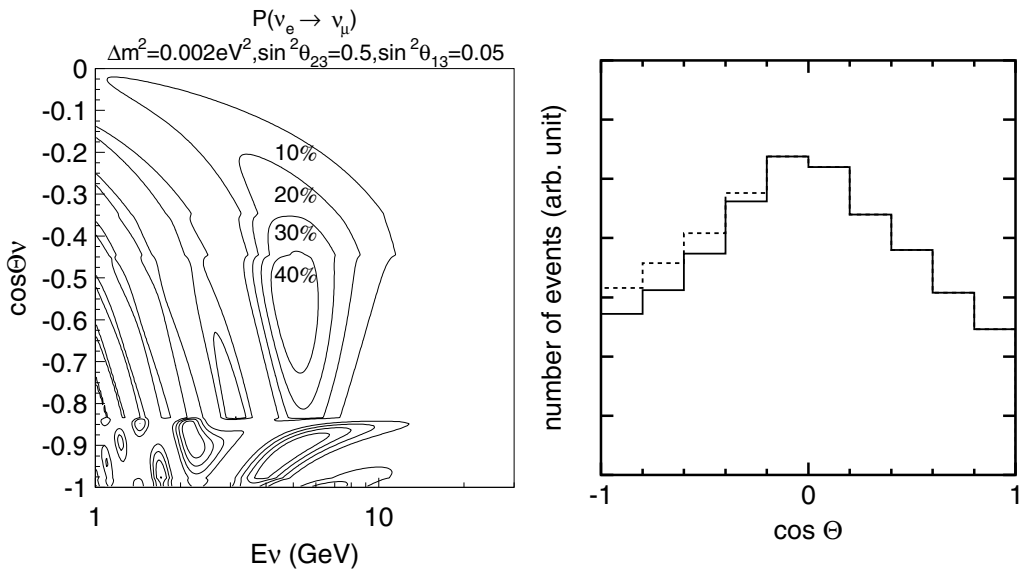

Figure 21. Left: $\nu_e \leftrightarrow \nu_\mu$ oscillation probability for neutrinos passing through the Earth as a function of the neutrino energy and zenith angle for $\Delta m^2_{23} = 2.0 \times 10^{-3}\,\mathrm{eV}^2$, $\sin^2\theta_{23} = 0.50$ and $\sin^2\theta_{13} = 0.05$. Right: expected zenith angle distribution for single + multi-ring e-like events in Super-Kamiokande with the observed energy between 2.5 and 5 GeV for oscillation with $\Delta m^2_{13} = 2.0 \times 10^{-3}\,\mathrm{eV}^2$, $\sin^2\theta_{23} = 0.50$ and $\sin^2\theta_{13} = 0.0$ (solid line histogram) and 0.05 (broken line histogram).

threshold effect of the τ production process which requires a ν_τ energy of at least 3.5 GeV to produce a τ lepton. These τ typically decay to hadrons (branching ratio is 64%) within 1 mm from the vertex point. These events should be upward-going but otherwise similar to energetic NC events, hence it is difficult to isolate ν_τ events in the on-going atmospheric neutrino experiments.

Super-Kamiokande has been searching for CC ν_τ events. The candidate ν_τ events were selected by a maximum likelihood or a neural network method. Various kinematical data were used as the inputs to the maximum likelihood or the neural network method. Even with these data, the signal-to-noise ratio was about 10%. However, the zenith-angle distribution can be used to estimate the number of ν_τ events statistically, because both the ν_τ signal and background events have accurately predicted zenith angle distributions. The best-fit numbers of ν_τ interactions that occurred in the fiducial volume of the detector during the 92 kt · year exposure were $145 \pm 44(\mathrm{stat.})^{+11}_{-16}(\mathrm{syst.})$, $99 \pm 39(\mathrm{stat.})^{+13}_{-21}(\mathrm{syst.})$ and $135^{+47}_{-44}(\mathrm{stat.}+\mathrm{syst.})$ events (preliminary) depending on the analysis [74]. The expected number was 86. The observed numbers of ν_τ interactions are consistent with the $\nu_\mu \rightarrow \nu_\tau$ expectation. The results are not statistically compelling, however they suggest that it may be possible in the near future to demonstrate the ν_τ interactions at more than 3σ level. At the time of writing, the Super-Kamiokande collaboration is finalizing the tau analysis.

5.9. Constraints on $\nu_\mu \leftrightarrow \nu_{\mathrm{sterile}}$ oscillations

An important question to ask is whether $\nu_\mu \leftrightarrow \nu_\tau$ oscillation is the only possible explanation of the atmospheric neutrino data. Since the observed effect is the energy- and zenith angle-dependent

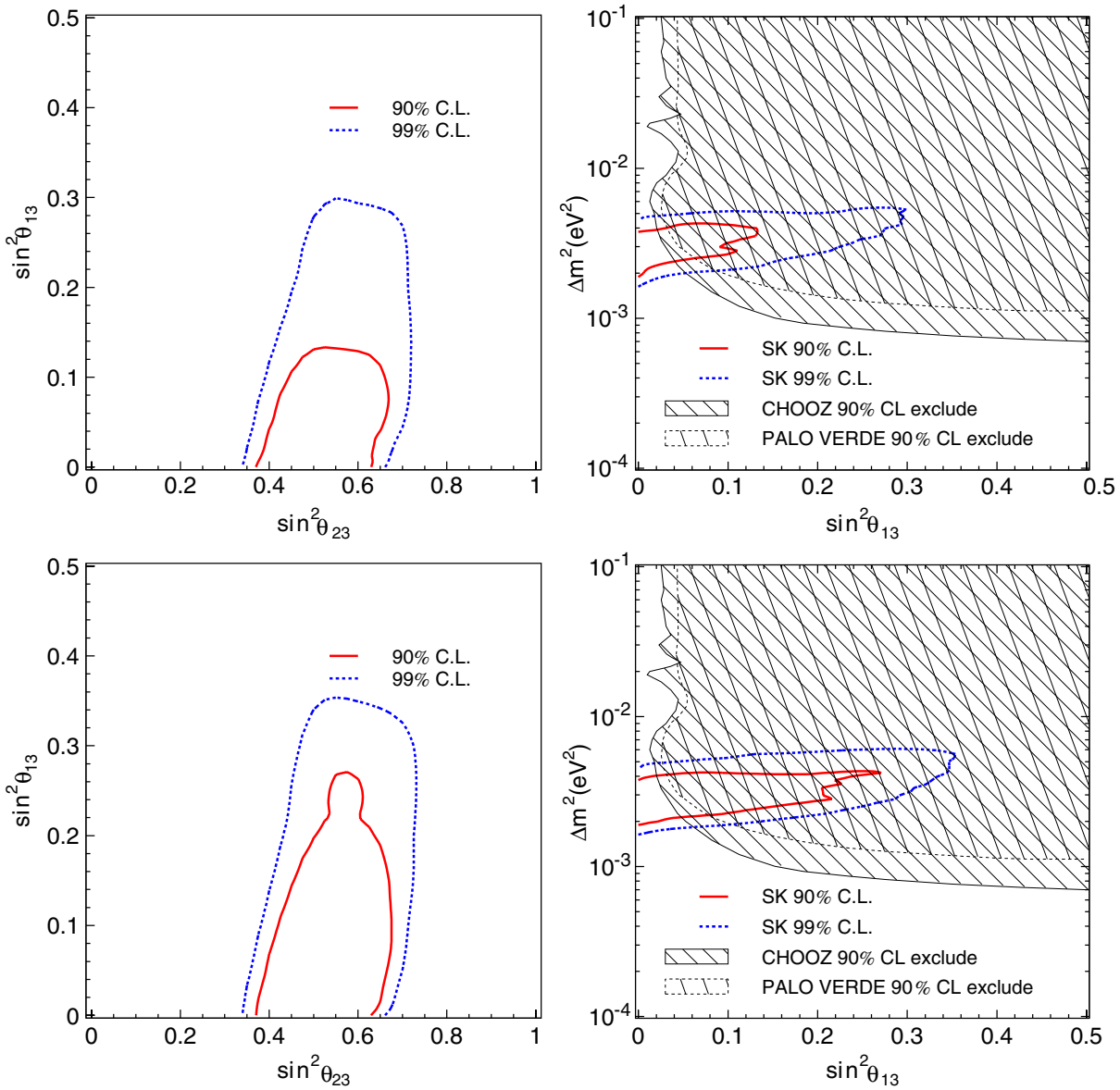

Figure 22. Allowed regions on the $\sin^2\theta_{23}$ and $\sin^2\theta_{13}$ plane (left) and the $\sin^2\theta_{13}$ and Δm^2_{23} plane (right) obtained by a three-flavour analysis of the Super-Kamiokande data (preliminary). Solid and dotted lines show the 90 and 99% CL allowed regions, respectively. Also shown in the right figures are the excluded regions by CHOOZ (shaded region) and Palo Verde (thin broken line in the shaded region) reactor experiments. The upper and lower panels are for positive and negative Δm^2_{23}, respectively.

deficit of CC ν_μ events, there have been several proposals for alternative explanations. One proposal was neutrino oscillations between ν_μ and ν_{sterile}, where ν_{sterile} is a neutrino-like particle that does not interact with matter by either CC or NC weak interactions. Since the deficit is seen for CC ν_μ events, $\nu_\mu \leftrightarrow \nu_{\text{sterile}}$ could explain the atmospheric neutrino data. Because the possible

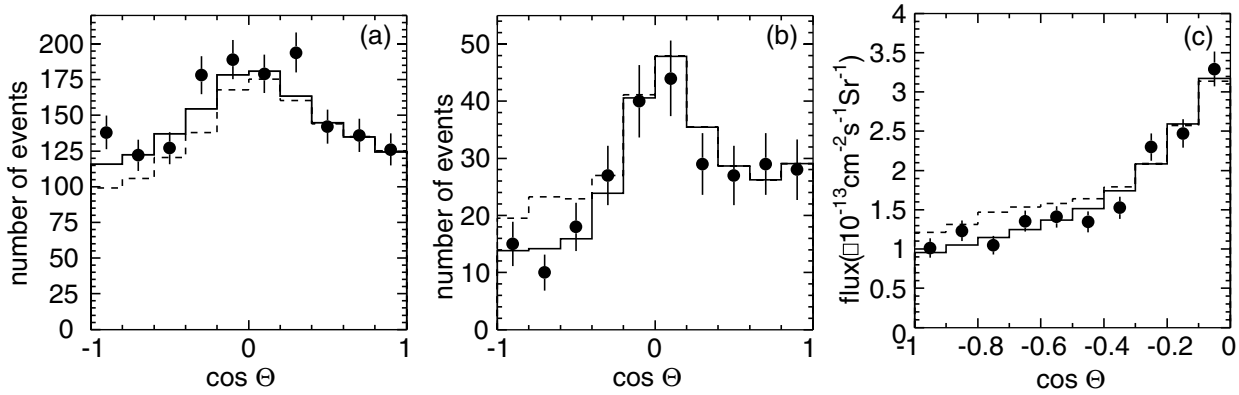

Figure 23. Zenith-angle distributions for: (a) multi-ring events with the most energetic ring being e-like and $E_{\rm vis} > 400$ MeV, (b) PC events with $E_{\rm vis} > 5$ GeV and (c) upward-through-going muon events [77]. The detector exposure was 70.5 kt · year for FC and PC events and 1138 days for upward-through-going muons. In these figures, solid (broken) histograms show predictions for $\nu_\mu \to \nu_\tau$ ($\nu_\mu \to \nu_{\rm sterile}$) oscillations with $\Delta m^2 = 3 \times 10^{-3}\,{\rm eV}^2$ and $\sin^2 2\theta = 1.0$. The predictions are normalized so that the numbers of observed and predicted events are equal at $0.4 < \cos\Theta < 1.0$ (for (a) and (b)) and $-0.4 < \cos\Theta < 0.0$ (for (c)).

existence of $\nu_{\rm sterile}$ has significant impact on particle physics and cosmology, it must be studied seriously whether $\nu_\mu \to \nu_{\rm sterile}$ oscillation is really favoured by the atmospheric neutrino data.

There are several ways to discriminate between the two possibilities. One possibility is to use a matter effect for upward going neutrino events [75, 76]. In the case of $\nu_\mu \to \nu_{\rm sterile}$ oscillations, the matter effect could change the oscillation probability significantly, while there is no change in the $\nu_\mu \to \nu_\tau$ oscillation probability. For $\Delta m^2 \sim (2\text{–}3) \times 10^{-3}\,{\rm eV}^2$, the oscillation probability is expected to be significantly different only for high-energy (>10–20 GeV) atmospheric neutrinos travelling through the Earth. In addition, the zenith-angle distribution for an NC-enriched sample is useful to discriminate between the two possibilities, because the NC events should be affected only for $\nu_\mu \to \nu_{\rm sterile}$ oscillations.

Super-Kamiokande analysed NC-enriched multi-ring, high-energy PC with $E_{\rm vis} > 5$ GeV, and upward-through-going muon events [77]. Multi-ring events with the most energetic ring being e-like and $E_{\rm vis} > 400$ MeV were used. The estimated fraction of NC events (in the absence of neutrino oscillations) was 29%. Figure 23 shows the zenith angle distributions for these samples. It is clear that all the data samples disfavour $\nu_\mu \to \nu_{\rm sterile}$ oscillations. Also, in MACRO, the zenith-angle distribution of upward-through-going muons was studied [78]. Pure $\nu_\mu \to \nu_{\rm sterile}$ oscillation has been excluded at more than 99% CL [77, 78].

Using all the atmospheric neutrino data from Super-Kamiokande, neutrino oscillations between ν_μ and ν_x have been studied, where ν_x is a mixed flavour state ($\cos\xi\nu_\tau + \sin\xi\nu_{\rm sterile}$) [79]. No evidence for a finite sterile neutrino component as a partner of the ν_μ oscillations has been observed. The upper limit on the $\nu_{\rm sterile}$ admixture is $\sin^2\xi < 0.20$ at 90% CL [50]. Very similar results based on the present data were obtained by various authors, see, for example, [80]. We, however, mention that the differences in the zenith angle distributions between $\nu_\mu \leftrightarrow \nu_\tau$ and $\nu_\mu \leftrightarrow \nu_{\rm sterile}$ are relatively small. Therefore it is important to control various systematic effects to

obtain stronger constraints on the ν_{sterile} admixture. Also, it is desirable to carry out a significantly different experiment on the ν_{sterile} admixture. One example is a long-baseline experiment to test the disappearance of NC events (such as single π^0 events) [81]. Finally, we stress that the detection of CC ν_τ interactions in future atmospheric or long-baseline experiments [82] will be further evidence against $\nu_\mu \leftrightarrow \nu_{\text{sterile}}$ oscillations.

5.10. Other interpretations

Possible non-standard neutrino interactions or properties can also generate neutrino oscillations. There have been several proposals for such mechanisms, such as neutrino oscillations generated by the violation of Lorentz invariance [83]. A list of possibilities can be found in [84]–[87]. We do not discuss the details of these models, although we mention that, in many such models, the energy dependence of the oscillation probability does not take the form $P(\nu_\mu \rightarrow \nu_\mu) = \alpha \sin(\beta L E_\nu^{-1})$, where α and β are constants. Instead, some of the models take the form, $P(\nu_\mu \rightarrow \nu_\mu) = \alpha \sin(\beta L E_\nu^n)$, where $n = 0$ or 1.

Since the atmospheric neutrino data cover the energy range from about 0.1 to 10^3 GeV, the energy dependence of the oscillation can be studied in detail. The Super-Kamiokande data (500 days of the detector exposure) were analysed in [85]. The data were fitted with n as a free parameter. It was found that $n = -0.9 \pm 0.4$ at 90% CL, thus essentially excluding non-standard oscillation models which take either $n = 0$ or 1. A similar conclusion was obtained in [84].

Some of the non-standard neutrino oscillations cannot be described by the above form. An important example of such a model is neutrino oscillations generated by flavour changing neutral currents (FCNC) [86]. In this case, the L/E_ν in the mass-generated neutrino oscillation is replaced by the column density. In this model, there is no energy dependence in the oscillations. Furthermore, since air has a density much lower than that of the Earth, down-going neutrinos are essentially unaffected. Therefore, the neutrino oscillation probability is a function of the zenith angle only. A detailed analysis of the atmospheric neutrino data in terms of FCNC was carried out in [84, 86, 87]. They observed that this model was essentially ruled out because, among other reasons, the observed upward-through-going muons had a deficit considerably smaller than the deficit of upward-going stopping muons and upward-going multi-GeV muons.

So far, we have assumed that the neutrino oscillation parameters are identical between neutrinos and anti-neutrinos. This assumption is correct under the CPT invariance. However, there are discussions that the neutrino oscillation parameters Δm^2_{ij} and θ_{ij} could be different between neutrinos and anti-neutrinos [88]. The Super-Kamiokande data have been analysed with different neutrino oscillation parameters for neutrinos and anti-neutrinos, resulting in no evidence for different neutrino and anti-neutrino oscillation parameters [50].

Finally, it should be mentioned that the recent L/E analysis from Super-Kamiokande [62] strongly disfavours these non-standard scenarios. With increasing data and improved analyses, it is getting clearer that $\nu_\mu \rightarrow \nu_\tau$ generated by neutrino mass is the dominant channel and that non-standard neutrino oscillations or flavour change does not contribute to the ν_μ deficit substantially [89].

6. Prospects of future atmospheric neutrino experiments

In addition to data described so far, unique data from several new experiments are expected to be available soon. SNO [63] is primarily a solar neutrino detector. However, because of the

great depth of the detector location (see figure 6), down-going muons near the horizon are due mostly to neutrino interactions. These neutrinos should have little oscillation effect, and should give very good calibration of the absolute neutrino flux at about 100 GeV neutrino energies. MINOS [90] is a detector designed primarily for accelerator long-baseline neutrino experiments. It has a magnetic field and can identify the charge of a long track. MINOS can make a unique contribution to atmospheric neutrino studies by measuring the μ^+/μ^- (or equivalently $\overline{\nu}_\mu/\nu_\mu$) ratio. ICARUS [91] is a 600 t liquid argon TPC. It will reconstruct events with unprecedented resolution. Although the mass of the detector is relatively small, high-resolution measurements of atmospheric neutrinos might give us unique information.

So far, there have been several considerations of future detectors that can improve our knowledge of neutrino masses and ixings through studies of atmospheric neutrinos. One type of the detectors is huge water Cherenkov detectors such as Hyper-Kamiokande [81] or UNO [92]. These detectors are assumed to have a mass of about 0.5–1 Mt. Another type of detectors is magnetized tracking detectors. Examples of such detectors are MONOLITH [93] and INO [94]. The masses for these detectors are assumed to be several tens of kt. The other possibility is a large liquid argon detector [91] with a mass similar to the other types of detectors and possibly a magnetic field inside the detector. We discuss below the physics potential of these atmospheric neutrino detectors.

6.1. Measurement of $\sin^2 2\theta_{23}$ *and* Δm^2_{23}

The mixing parameters, θ_{ij}, are one of a few fundamental parameters that could constrain theories beyond the standard model of particle physics. Therefore, it is important to measure $\sin^2 2\theta_{23}$ as accurately as possible. The atmospheric neutrino flux is accurately predicted to be up–down symmetric in the multi-GeV energy range. The numbers of downward- and upward-going ν_μ events and $\sin^2 2\theta_{23}$ are related by $(up/down)_{\rm Data}/(up/down)_{\rm MC} \simeq 1 - (\sin^2 2\theta_{23})/2$ to first approximation, assuming that there is no (full) oscillation effect for downward (upward)-going neutrinos. The systematic error in the up–down ratio measurement is about 1% in the present Super-Kamiokande experiment [44]. Hence atmospheric neutrino data are useful for an accurate measurement of $\sin^2 2\theta_{23}$. The accuracy of the $\sin^2 2\theta_{23}$ measurement will be improved with (exposure time)$^{1/2}$ and will be about $\pm 2\%$ at 1σ for 1 Mt $\cdot$ year exposure of a water Cherenkov detector 95.

Super-Kamiokande has shown that Δm^2_{23} can be measured accurately by measuring a dip in the L/E distribution [62]. It is difficult to predict the general sensitivity as a function of the detector exposure. Especially, in the case of water Cherenkov detectors, the sensitivity strongly depends on the true Δm^2_{23} value, because the dip moves to a lower L/E position (i.e., a higher neutrino energy for the same L) for a higher Δm^2_{23}. The number of events decreases for higher energy neutrinos. In addition, the acceptance for fully contained events decreases for higher energy neutrinos. Hence, the sensitivity in Δm^2_{23} gets worse rapidly with higher Δm^2_{23}. We, however, note that large atmospheric neutrino experiments could compete in the Δm^2_{23} measurement with future long-baseline neutrino experiments if the true Δm^2_{23} value is near the lower edge of the presently allowed Δm^2 region, where the planned long-baseline experiments have somewhat limited sensitivities. A few per cent measurement of Δm^2_{23} is possible with more than 1 Mt $\cdot$ year exposure of a large water Cherenkov detector, if the true Δm^2_{23} is smaller than 2.0×10^{-3} eV^2 [96].

6.2. θ_{13}

The effect of a non-zero θ_{13} could be observed as an excess of ν_e events in the upward-going direction through the matter resonance effect in the multi-GeV energy range (see figure 21). The sensitivity to θ_{13} of a large water Cherenkov detector was discussed in detail in [96]. If $\theta_{23} = 45^\circ$, as 3 SD sensitivity is about $\sin^2 2\theta_{13} > 0.02$ for 450 kt · year exposure. The chance of observing finite θ_{13} rapidly improves for larger $\sin^2 \theta_{23}$ [97]. Also, the sensitivity does not depend strongly on Δm^2_{23}. Finally, it should be mentioned that finite θ_{13} could make it possible to discriminate $\theta_{23} > 45^\circ$ and $< 45^\circ$.

6.3. *Sign of* Δm^2

The resonance effect occurs only for neutrinos for positive Δm^2 and, therefore, only appears for the e^- and μ^- spectrum. This, in turn, suggests that the sign of Δm^2_{23} could be measured by atmospheric neutrino experiments. It is generally believed that a massive magnetized detector, which can measure the charge of muons, is necessary to measure the sign of Δm^2_{23} [93]. With a 200 (400) kt · year exposure, it will be possible to determine the sign of Δm^2 at 90% CL if $\sin^2 2\theta_{13} > 0.1$ (0.05).

Super-Kamiokande and other water Cherenkov detectors are unable to distinguish ν_e and $\overline{\nu}_e$ interactions on event-by-event basis. However, the cross section and the y $(=(E_\nu - E_{\text{lepton}})/E_\nu)$ dependence of the cross section are different between ν and $\overline{\nu}$ and, therefore, it may be possible to distinguish the positive and negative Δm^2_{23}. For positive Δm^2_{23}, the resonance effect occurs only for neutrinos. Since the neutrino interactions produce more high-y events (i.e., more multi-hadron events) than the anti-neutrino interactions, a larger effect of the finite θ_{13} can be seen in multi-ring e-like events for positive Δm^2_{23} than for negative Δm^2_{23}. Detailed Monte Carlo studies showed that it is possible to measure the sign of Δm^2_{23} in water Cherenkov detectors, if the $\sin^2 \theta_{13}$ and $\sin^2 \theta_{23}$ values are near the present limit ($\sin^2 2\theta_{13} > (0.01\text{–}0.02)$) and $\geqslant 0.5$, respectively, provided that the detector exposure is >1 Mt · year [96].

6.4. *Effects of the solar oscillation terms*

The present analyses of the atmospheric neutrino data do not include the oscillation terms that are related to solar neutrinos (θ_{12} and Δm^2_{12}). It has been pointed out that these terms (and the interference terms between the terms related to θ_{13} and θ_{12}) could play a unique role in the atmospheric neutrino oscillations, such as the possible measurement of $\sin^2 \theta_{23}$ (i.e., the discrimination of $\theta_{23} > 45^\circ$ and $<45^\circ$) [66, 67]. These effects have been studied by taking various systematic errors into account [98].

7. Summary

Atmospheric neutrinos have played essential roles in the discovery of neutrino oscillations and are still contributing significantly to the study of neutrino oscillations. The atmospheric neutrino data from various experiments are well explained by $\nu_\mu \to \nu_\tau$ oscillations. Many proposed non-standard explanations have been excluded by detailed studies of the high statistics atmospheric neutrino data. In particular, recent L/E analysis from Super-Kamiokande gives the first direct evidence that the neutrino survival probability obeys the sinusoidal function

as predicted by neutrino oscillations. The 90% CL allowed region of neutrino oscillation parameters from the Super-Kamiokande's L/E analysis is: $1.5 \times 10^{-3} < \Delta m^2_{23} < 3.4 \times 10^{-3}\,\mathrm{eV}^2$ and $\sin^2 2\theta_{23} > 0.92$. Atmospheric neutrino experiments are also sensitive to θ_{13}. However, no evidence for non-zero θ_{13} has been observed.

Although the present atmospheric neutrino data are explained by $\nu_\mu \rightarrow \nu_\tau$ oscillations, there are several open questions. These questions must be addressed in future neutrino oscillation experiments including atmospheric neutrino and long-baseline neutrino oscillation experiments. Especially, it would be possible for the future atmospheric neutrino experiments to measure the $\sin^2 2\theta_{23}$ and Δm^2_{23} values precisely, to observe a non-zero θ_{13} and to determine the sign of Δm^2_{23}, if the true θ_{13} is relatively large. The study of neutrino oscillations will continue to be an important and exciting field and atmospheric neutrino experiments are likely to contribute to this field substantially.

Acknowledgments

We gratefully acknowledge the members of the Super-Kamiokande collaboration for useful discussions and information. This work was partially supported by the Japanese Ministry of Education, Culture, Sports, Science and Technology and the Japan Society for the Promotion of Science.

References

[1] Yanagida T 1979 *Proc. Workshop Unified Theory and Baryon Number in the Universe (KEK report 79-18)* ed O Sawada and A Sugamoto, p 95
[2] Gell-Mann M, Lamond P and Slansky R 1979 *Supergravity* ed P van Nieuwenhuizen and D Z Freedman (Amsterdam: North-Holland) p 315
[3] Pati J C and Salam A 1973 *Phy. Rev. Lett.* **31** 661
[4] Georgi H and Glashow S L 1974 *Phy. Rev. Lett.* **32** 438
[5] Maki Z, Nakagawa M and Sakata S 1962 *Prog. Theor. Phys.* **28** 870
[6] Pontecorvo B 1967 *Zh. Eksp. Teor. Fiz.* **53** 1717
Pontecorvo B 1968 *Sov. Phys.—JETP* **26** 984 (Engl. transl.)
[7] Eidelman S *et al* (Particle Data Group) 2004 *Phys. Lett.* B **592** 1
[8] Achar C V *et al* 1965 *Phys. Lett.* **18** 196
Achar C V *et al* 1965 *Phys. Lett.* **19** 78
Krishnaswamy M R *et al* 1971 *Proc. R. Soc.* A **323** 489
[9] Reines F *et al* 1965 *Phys. Rev. Lett.* **15** 429
[10] Crouch M F *et al* 1978 *Phys. Rev.* D **18** 2239
[11] Haines T J *et al* 1986 *Phys. Rev. Lett.* **57** 1986
[12] Nakahata M *et al* 1986 *J. Phys. Soc. Japan* **55** 3786
[13] Hirata K S *et al* 1988 *Phys. Lett.* B **205** 416
[14] Casper D *et al* 1991 *Phys. Rev. Lett.* **66** 2561
Becker-Szendy R *et al* 1992 *Phys. Rev.* D **46** 3720
[15] Aglietta M *et al* 1989 *Europhys. Lett.* **8** 611
[16] Berger Ch *et al* 1989 *Phys. Lett.* B **227** 489
Berger Ch *et al* 1990 *Phys. Lett.* B **245** 305
[17] Daum K *et al* 1995 *Z. Phys.* C **66** 417
[18] Fukuda Y *et al* 1994 *Phys. Lett.* B **335** 237

[19] Fukuda Y *et al* 1998 *Phys. Rev. Lett.* **81** 1562
[20] Honda M, Kajita T, Kasahara K and Midorikawa S 2004 *Phys. Rev.* D **70** 043008
[21] Barr G *et al* 2004 *Phys. Rev.* D **70** 023006
[22] Battistoni G, Ferrari A, Montaruli T and Sala P R 2003 *Preprint* hep-ph/0305208
[23] Gaisser T K and Honda M 2002 *Ann. Rev. Nucl. Part. Sci.* **52** 153
[24] Honda M, Kajita T, Kasahara K and Midorikawa S 1995 *Phys. Rev.* D **52** 4985
[25] Agrawal V, Gaisser T K, Lipari P and Stanev T 1996 *Phys. Rev.* D **53** 1314
[26] Alcaraz J *et al* 2000 *Phys. Lett.* B **490** 27
[27] Sanuki T *et al* 2000 *Astrophys. J.* **545** 1135
[28] Battistoni G *et al* 2000 *Astropart. Phys.* **12** 315
[29] Lipari P 2000 *Astropart. Phys.* **14** 153
[30] Lipari P 2001 *Nucl. Phys.* B *(Proc. Suppl.)* **81** 159
[31] Llewellyn Smith C H 1972 *Phys. Rep.* **3** 261
[32] Smith R A and Moniz E J 1972 *Nucl. Phys.* B **43** 605
[33] Rein D and Sehgal L M 1981 *Ann. Phys.* **133** 79
[34] Rein D and Sehgal L M 1983 *Nucl. Phys.* B **223** 29
[35] Perkins D H 1984 *Ann. Rev. Nucl. Part. Sci.* **34** 1
[36] Becker-Szendy R *et al* 1993 *Nucl. Instrum. Methods* A **324** 363
[37] Nakamura K *et al* 1994 *Physics and Astrophysics of Neutrinos* ed M Fukugita and A Suzuki (Berlin: Springer) p 249
[38] Fukuda Y *et al* 2003 *Nucl. Instrum. Methods* A **501** 418
[39] Battistoni G *et al* 1986 *Nucl. Instrum. Methods* A **245** 277
[40] Berger Ch *et al* 1987 *Nucl. Instrum. Methods* A **262** 463
[41] Allison W W M *et al* 1996 *Nucl. Instrum. Methods* A **376** 36
Allison W W M *et al* 1996 *Nucl. Instrum. Methods* A **381** 385
[42] Alekseev E N *et al* 1998 *Phys. Part. Nucl.* **29** 254
[43] Ahlen S P *et al* 1993 *Nucl. Instrum. Methods* A **324** 337
Ambrosio M *et al* 2002 *Nucl. Instrum. Methods* A **486** 663
[44] Super-Kamiokande Collaboration 2004, in preparation
[45] Giorgini M (for the MACRO collaboration) 2002 *Proc. 3rd Int. Conf. on Particle Physics Beyond the Standard Model: Accelerator, Non-Accelerator and Space Approaches (Oulu, Finland, June 2002)*, ed H V Klapdor-Kleingrothaus p 353
[46] Hirata K S *et al* 1992 *Phys. Lett.* B **280** 146
[47] Allison W W M *et al* 1999 *Phys. Lett.* B **449** 137
[48] Clark R *et al* 1997 *Phys. Rev. Lett.* **79** 345
[49] Mann W A, Kafka T and Leeson W 1992 *Phys. Lett.* B **291** 200
[50] Kearns E, for the Super-Kamiokande Collaboration 2004 talk presented at the *XXI Int. Conf. on Neutrino Physics and Astrophysics (Neutrino 2004, Paris, June 2004)*
[51] Sanchez M *et al* 2003 *Phys. Rev.* D **68** 113004
[52] Ambrosio M *et al* 2004 *Eur. Phys. J.* C **36** 323
[53] Giacomelli G *et al* 2004 *Phys. Atom. Nucl.* **67** 1139
[54] Fogli G L *et al* 2002 *Phys. Rev.* D **66** 053010
[55] Hatakeyama S *et al* 1998 *Phys. Rev. Lett.* **81** 2016
[56] Ahn M H *et al* 2003 *Phys. Rev. Lett.* **90** 041801
[57] Nakaya T, for the K2K Collaboration 2004 talk presented at the, *XXI Int. Conf. on Neutrino Physics and Astrophysics (Neutrino 2004, Paris, June 2004)*
[58] Barger V D *et al* 1999 *Phys. Lett.* B **462** 109
[59] Grossman Y and Worah M P 1998 *Preprint* hep-ph/9807511
[60] Lisi E, Marrone A and Montanino D 2000 *Phys. Rev. Lett.* **85** 1166
[61] Ambrosio M *et al* 2003 *Phys. Lett.* B **566** 35

[62] Ashie Y *et al* 2004 *Phys. Rev. Lett.* **93** 101801
[63] Ahmed S N *et al* 2004 *Phys. Rev. Lett.* **92** 181301
[64] Smy M B *et al* 2004 *Phys. Rev.* D **69** 011104
[65] Araki T *et al* 2004 *Preprint* hep-ex/0406035
[66] Peres O L G and Smirnov Y Au 1999 *Phys. Lett.* B **456** 204
[67] Peres O L G and Smirnov Y Au 2004 *Nucl. Phys.* B **680** 479
[68] Mikheyev S P and Smirnov A Yu 1985 *Sov. J. Nucl. Phys.* **42** 1441
Mikheyev S P and Smirnov A Yu 1986 *Nuovo Cimento* C **9** 17
[69] Wolfenstein L 1978 *Phys. Rev.* D **17** 2369
[70] Fogli G L *et al* 1997 *Phys. Rev.* D **55** 4385
[71] Giunti C, Kim C W and Monteno M 1998 *Nucl. Phys.* B **521** 3
[72] Apollonio M *et al* 1999 *Phys. Lett.* B **466** 415
[73] Boehm F *et al* 2001 *Phys. Rev.* D **64** 112001
[74] Saji C, for the Super-Kamiokande Collaboration 2003 *Proc. 28th Int. Cosmic Ray Conf. (Tsukuba)* vol 3, ed T Kajita *et al* p 1267
[75] Liu Q Y, Mikheyev S P and Smirnov A Yu 1998 *Phys. Lett.* B **440** 319
[76] Lipari P and Lusignoli M 1998 *Phys. Rev.* D **58** 073005
[77] Fukuda S *et al* 2000 *Phys. Rev. Lett.* **85** 3999
[78] Ambrosio M *et al* 2001 *Phys. Lett.* B **517** 59
[79] Fogli G L, Lisi E and Marrone A 2001 *Phys. Rev.* D **63** 053008
[80] Maltoni M, Schwetz T, Tortola M and Valle J W F 2004 *Preprint* hep-ph/0405172
[81] Itow Y *et al* 2001 *Preprint* hep-ex/0106019
[82] Rubbia A 2001 *Nucl. Phys.* B *(Proc. Suppl.)* **91** 223
[83] Coleman S R and Glashow S L 1997 *Phys. Lett.* B **405** 249
[84] Lipari P and Lusignoli M 1999 *Phys. Rev.* D **60** 013003
[85] Fogli G L *et al* 1999 *Phys. Rev.* D **60** 053006
[86] Gonzalez-Garcia M C *et al* 1999 *Phys. Rev. Lett.* **82** 3202
[87] Fornengo N, Gonzalez-Garcia M C and Valle J W F 2000 *J. High Energy Phys.* JHEP07(2000)006
[88] Barenboim G, Borissov L, Lykken J and Smirnov A Yu 2002 *J. High Energy Phys.* JHEP210(2002)001
[89] Fornengo N, Maltoni M, Tomas Bayo R and Valle J W F 2002 *Phys. Rev.* D **65** 013010
[90] Michael D 2003 *Nucl. Phys. (Proc. Suppl.)* **118** 189
[91] Arneodo F *et al* 2001 *Nucl. Instrum. Methods* A **461** 324
[92] Jung C K 2000 *Preprint* hep-ex/0005046
[93] Tommaso Tabarelli de Fatis 2001 *Proc. La Thuile 2001, Results and Perspectives in Particle Physics (La Thuile, Italy)* p 677 (*Preprint* hep-ph/0106252)
[94] Rajasekaran G 2004 *Preprint* hep-ph/0402246
[95] Kajita T, for the Super-Kamiokande Collaboration 2001 *Nucl. Phys.* B *(Proc. Suppl.)* **100** 139
[96] Kajita T 2004 talk presented at the *5th Workshop on Neutrino Oscillations and their Origin (NOON 2004, Tokyo, February 2004)*
[97] Bernabeu J, Palomares-Ruiz S and Petcov S T 2003 *Nucl. Phys.* B **669** 255
[98] Gonzalez-Garcia M C, Maltoni M and Smirnov A Yu 2004 *Preprint* hep-ph/0408170